MODELING OF AN AEROSPACE SAND CASTING PROCESS

A Thesis:

submitted to the Faculty

of the

WORCESTER POLYTECHNIC INSTITUTE

in partial fulfillment of the requirements for the

Degree of Master of Science
In
Materials Science and Engineering

by

Joseph E. Ziolkowski

December, 2002

APPROVED:

_____
Diran Apelian, Material Science and Engineering, Advisor

_____

Richard D. Sisson Jr., Material Science and Engineering, Program Head

1. **modeling**
2. **casting**
3. **sand**

Abstract

Theoretical issues relating to the aerospace sand casting simulation are laid out, identifying parameters used in the model. A sensitivity analysis is performed to examine the mold-metal heat transfer coefficient, mold thermal conductivity, wall friction factor, pouring basin pour temperature, and pouring basin head pressure through doing coupled flow simulations on thin-walled castings using the commercial casting simulation software, MAGMASOFT®. A verification exercise is done to match simulation with reality with the knowledge that mold-metal heat transfer coefficient and mold thermal conductivity are the most influential parameters of the five. Validation on a real production casting is performed using the tuned parameters from the verification exercise.

Acknowledgements

Special thanks are given to the following organizations and personnel for their contributions to this project:

Diran Apelian, for his advice and encouragement throughout this project,
Hitchcock Industries, for the use of their facilities, equipment and resources,
Dinshaw Irani, for his aerospace sand casting knowledge,
Tom Vick, for his aerospace sand casting knowledge and simulation involvement,
Joe Hirvela, for his aerospace sand casting knowledge and experimental technique,
Thomas McKeown, for his engineering support in casting simulation research.
Dr. Charles Bates, Preston Scarber Jr., and John Griffin, from the University of Alabama at Birmingham, for their cooperation with Hitchcock Industries in the field of simulation of aerospace sand casting processes.

Table of Contents

List of Figures

Preface

The scope of this report is to provide information to the aerospace industry relating to computational simulation of the sand casting process. A practical method of strategically accomplishing the task of accurately performing simulations is presented, giving examples using practical foundry methods, materials and equipment. Since all activities were undertaken at the foundry, an emphasis on real-world practicality encompasses this report.

1. Introduction

Hitchcock Industries has been producing complex, premium aluminum and magnesium sand castings for the aerospace industry since 1916. Until now, much of the success of Hitchcock's engineering has been due to the accumulated practical foundry knowledge over the past 85 years of doing business. The design of sand molds, which produce castings with high geometric complexity and material properties, has largely been a "reactive engineering" endeavor. Typically, mold designs go through iterations before a final configuration is achieved. Much of this is due to the complexity of the process itself; and engineers in this industry are continuously gaining more insight into control of the key variables every day largely through focused experimentation and experience.

An ideal aerospace foundry situation would be to control all the key influential process variables to design a mold robust enough that would produce castings to the required specifications—the first time and every time after that.

One way to examine process variables and to determine their influence on the final product is through the use of computational simulation. In the past, this has not been an option simply because the high geometric and material complexity of aerospace castings made simulation results painstakingly slow regardless of the hardware used. Any information gathered was too late to meet the short lead times required for product development. Also, many of the materials used by aerospace sand foundries are not widely used by those who are familiar with casting simulation, and material properties are not rigorously

established. As a result, aerospace sand foundry engineering has continued to rely on vast past experiences, standard gating practices and in-house knowledge base of pattern and gating shops. This has demonstrated to serve them with the ability to develop the most complex sand castings in the world. Adding casting simulation to the toolbox would only increase the aerospace foundryman's edge on complex casting development.

It is now believed that computational capabilities have reached a point to where this complex casting process and geometry can be modeled in a reasonable amount of time and effort. There is also a greater pool of knowledge with regard to interface heat transfer coefficients (HTC) between light alloys and sand molds and solidification behavior. However, there are unknowns to be resolved when addressing many of the unique issues in aerospace sand casting. Hopefully, with these topics resolved, the aerospace sand foundry will be able to model its casting process in an accurate and timely manner; allowing proactive optimization of robust mold designs. In the future, this new tool will allow the aerospace foundry engineer to reduce design iteration, and optimize gating, risering, and chilling in these complex castings.

The aim of this project is to investigate the key parameters that are most influential for this process, and to continually improve their values for use in industry. Specifically, to identify the key process parameters that significantly affect the sand casting process, and examine their sensitivity. Also, a verification and validation is performed for comparison to reality utilizing MAGMASOFT®,

commercially available casting simulation software. Ultimately, this will lead to the fine tuning of key parameters, more accurately representing reality.

2. Background

The key to obtaining a casting simulation representative of reality is to study all the key controllable influential parameters in the model and to allocate their respective contributions to simulation results. These parameters can be classified into two categories. The first is the database of material thermophysical properties. These are data that describe the characteristic behavior of the material regarding heat transfer coupled with fluid flow. These values are unique for certain materials and in many cases are results of the methods by which the materials are produced. The second category is the casting interfacial boundary conditions. In a simulation, the user must set the initial pour temperature and flow conditions at the inlet, or melt entry point into the system. Unless these values are known within a reasonable tolerance, results will be inconsistent with reality. The best method for determining inlet temperature is to place a thermocouple and directly measure the temperature during the pour at inlet locations to obtain the temperature losses from the pot to the inlet. Once the importance of a particular variable is known, an experimentally measured quantitative description of that parameter can be obtained. When attempting to model a sand casting process, there are many parameters involved and are given as:

Alloy/Mold Heat Transfer Coefficient (HTC)

Mold Material Thermal Properties

Flow Boundary Condition

Inlet Boundary Conditions

Filter Parameters

Alloy Thermal Properties

Chill Thermal Properties

Insulation Thermal Properties

Alloy/Chill Heat Transfer Coefficient

Alloy/Insulation Heat Transfer Coefficient

Alloy Feeding Characteristics

Chill/Mold Heat Transfer Coefficient

Insulation/Mold Heat Transfer Coefficient

Mold Permeability

Metal Front Surface Tension

The bold parameters in the above list were selected for investigation since they are the more significant ones. In the next section, each parameter is addressed, and physical importance as well as computational modeling strategy is described. All of these parameters are existent in the MAGMASOFT® commercial casting simulation software code[7].

2.1 Thermophysical Data

2.1.1 Mold-Metal Heat Transfer Coefficient

The main controlling factor in the solidification/heat transfer of sand castings is the insulating properties of the mold. This is true for the majority of the total solidification time; however at the very beginning of solidification, when molten metal near the liquidus temperature first comes in contact with the mold surface, heat transfer is controlled at the mold-metal interface. The main parameter that models this phenomenon is the interfacial heat transfer coefficient (HTC). The HTC can be expressed as follows.

$$q_{m/c} = h_{m/c}\left(T_c - T_m\right) \qquad (1)$$

In the above equation, q is the heat flux per unit area, $h_{m/c}$ is the mold/casting interfacial HTC in units of $\frac{\text{heat flux}}{\text{area} * \text{temperature}}$. T_c is the temperature at the casting side of the interface and T_m is the temperature at the mold side of the interface. This mode of heat transport is commonly used when talking about interfaces and convection. But once the metal begins to solidify at the mold/casting interface it is no longer a fluid. Figure 1 a-d illustrates the condition of this interface as solidification is initiated. Figure 1a shows the temperatures of the metal and mold at t=0. It should be noted that the instant that the metal comes in contact with the mold, the mold temperature and the metal temperature

are not the same. Some infinitesimal time later, t>0, the mold temperature and the casting temperature come closer to each other, but there may still be a difference. Once the metal arrives at the liquidus temperature, solidification will commence via a nucleation and growth process. In Figure 1c, the interface temperature has reached the solidus marking the first complete solid to form. Note that throughout this process, the schematic temperature profiles in the mold and metal never match at the interface. This can be physically explained by discussing the small air gap, or discontinuity, that exists at the mold metal interface throughout the entire solidification process. This air gap exists due to metal contraction upon solidification and the gap size depends strongly upon the casting geometry. If there was no air gap, there would be an intimate contact between mold and metal and the HTC would be a higher number than if there was a large air gap.

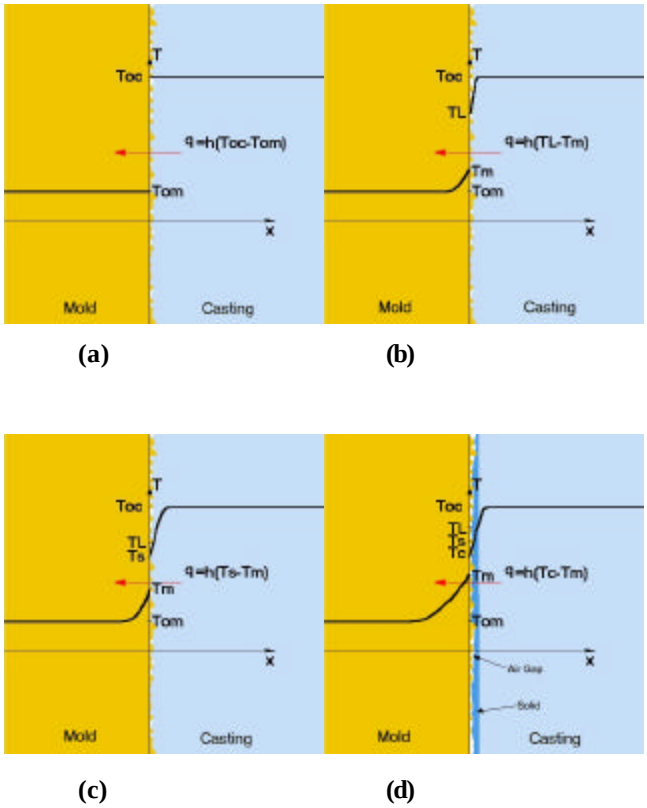

Figure 1(a-d): Schematic temperature profiles

In reality, an air gap exists to some degree, and consequently, quite a low HTC exists compared to a casting-chill contact. The question is, whether the HTC is low enough that it controls heat transfer, or the thermal conductivity of the mold is the controlling factor. One can observe and quantify this "competition for control" through the non-dimensional Biot (Bi) number.

The Biot number is given as

$$Bi = \frac{hL}{k} \qquad (2)$$

where h is the interfacial heat transfer coefficient, k is the thermal conductivity of the mold, and L is a characteristic length or the perpendicular distance from the mold metal interface. Equation 4 shows the ratio of interface controlled heat transfer to diffusion controlled heat transfer. If Bi=1, the interfacial effects are about equal to the diffusion effects. If Bi<0.1, we can estimate interfacial effects to be greater than diffusion effects by a factor of ten. Typically, HTC values around 500 $\frac{W}{m^2K}$ and k values of 0.6 $\frac{W}{mK}$ produce a Bi of 833*L. So, depending on the casting wall thickness, various different modes of heat transfer control the solidification journey. For thin-walled, aerospace sand castings, typical wall thicknesses can be as small as 0.09" or 0.00229m. A one-dimensional semi-infinite model of heat transfer produces a characteristic length 0.00115m and a Bi=0.954. It should be pointed out that both h and k can vary throughout solidification. If high thermal conductivity sand is used, a realistic k value is 1.0 $\frac{W}{mK}$. Furthermore, any mold-insulating materials used will further lower the mold-metal HTC. So Bi could be slightly higher and significantly lower than 0.954. From this primary physical and geometric

investigation, the HTC is an important parameter in the solidification of thin-walled sand castings and in some instances can be the controlling parameter in heat transfer.

To date, there is little rigorously established data available involving mold metal HTC's simply because for most sand casting processes, a precise HTC description is not necessary for achieving adequate results. The sand-metal HTC is also an extremely difficult parameter to experimentally measure. The HTC is slightly different for every alloy-mold combination. Approximations in the mold-metal HTC are made all the time and results show that through matching solidification simulations with reality, the HTC between a silica sand mold and aluminum alloy has been found to lie in the range of 500-1500 $\frac{W}{m^2 K}$.

2.1.2 Carbon Black

Carbon black, or acetylene black, is a byproduct of the combustion of acetylene gas and is commonly known and referred to as soot in the foundry. Soot becomes a very powerful tool when applied to the mold cavity surface in regions where thin walls of a mold exist as a preventative measure against misruns. Although there has been some debate on how carbon black makes its contribution towards reducing misruns, the majority of people investigating this phenomenon believe it affects the heat transfer of the system, reflected in the HTC. The thought here is carbon black acts as an insulating layer between the molten metal and mold. The layer slows heat transfer and improves the filling of the metal, allowing the metal to flow further into thin-walled regions thereby reducing misruns. Another factor is that the surface tension between the metal and a mold surface coated with carbon black reduces flow resistance allowing the metal front to advance with greater ease.

2.1.3 Alloy Thermal Properties

Most commercial casting simulation packages solve the equations of heat and momentum transfer in order to produce solidification results. With this being the case, the most important simulation parameters are those which control heat and momentum transfer. For coupled heat and momentum transfer, the important alloy parameters are the metal kinematic viscosity, u, density, r, specific heat, c_p, thermal conductivity, k, latent heat, L, and solid fraction, f_s. All of these parameters are a function of temperature and must be experimentally determined in one way or another. Some of these properties don't change appreciably from one alloy composition to another, allowing the parameter to be generalized to a certain class of alloys. Viscosity is one of these parameters, however the point at which the molten metal becomes solid and the equations of momentum no longer apply is different for each individual alloy. This would be reflected in $f_s = f_s(T)$ where T is the solidus temperature. Each alloy composition will have a distinctly different solidus temperature. The main objective is to discern which parameters must be determined and which can be generalized and what is the acceptable deviation from the actual values.

2.1.4 Mold Thermal Properties

Properties of concern for the mold material are the same for the alloy, but there are no momentum transfer quantities to deal with since the mold is in a solid state. If these parameters examined along with the HTC and alloy thermal properties, we can observe interactions between parameters of the mold and the alloy. For instance, if the thermal conductivity of the mold is the same as the thermal conductivity of the metal, $k_{mold} = k_{metal}$, the Bi would be a very low number and heat transfer would be almost exclusively

governed by the HTC. However, sand mold thermal conductivities have been experimentally measured and they are significantly lower than the alloy thermal conductivity. This places the mold thermal conductivity high on the list of controlling heat transfer in the sand casting process.

Values for mold thermal conductivity have been obtained using the Laser Flash Diffusivity method in a laboratory setting [4]. Preliminary simulation efforts were conducted at Hitchcock Industries and the University of Alabama at Birmingham with several interesting findings. First, mold material properties as determined in the laboratory are different from one sand-binder system to another, and have to be modified to correctly represent what is being used in the foundry. Second, the laboratory method of measuring sand thermal conductivity is very different from what the mold experiences during the casting process, and may not adequately describe the transport of energy out of the metal in the real casting process. When metal is poured into a mold, not only is heat transfer occurring as a mode of energy transport, but also heat is being used to break down binder material at a certain rate. In order to correctly describe heat transfer as it happens in the casting process, there has to be some way to account for the chemical reaction of heat breaking down the binder and hot gasses travelling through the sand grains and out of the mold. Since commercial codes don't have this capability as of yet, the easiest solution may be to include these effects into the thermal conductivity parameter.

2.1.5 Filter Parameters

The purpose of the filter is to remove particulate melt inclusions from the melt prior to casting. These inclusions/impurities encountered by the filter are the result of many actions including but not limited to alloying practices, degassing/fluxing techniques, and

initial turbulence in the mold prior to contact with the filter. Not only does the filter provide a way of mechanically intercepting impurities that were in existence before contact with the filter, but it also controls flow behavior, reducing erratic flow upon passing. It is the latter purpose of the filter that is desirable to model due to the large direct consequences erratic, eddying melt flow has on dross formation and mechanical properties.

Not only are differences noted when a filter has and has not been used, they are even noted when two filters are compared having the same specifications, but made by different manufacturers/processes. One ceramic foam filter with 20 pores per inch (ppi) may show very different flow resistance characteristics than another 20 ppi filter made by different manufacturer. For this reason, it is important to characterize the ceramic foam filter by the factors, which we wish to observe change in the simulation. A physical way of looking at the filter's contribution to flow behavior is a porous medium through which flow occurs and is given as.

$$\frac{\Delta P}{L} = \frac{m}{k_1} U \qquad (3)$$

At low velocities, ceramic foam filters behave according to Darcy's Law for flow through porous media [5,6]. Above, ΔP is the pressure drop across a medium of length L. The constant k_1 is the specific permeability, or the Darcian permeability, and is a function of porosity and pore size. m is the fluid viscosity which travels at an average velocity, U. At higher velocities, the pressure drop across a filter of thickness, L, is not linear with U but experiences a quadratic variation with the flow. This is due to the inception of inertial effects inducing additional resistance by the filter. These effects on the pressure drop have experimentally shown to exhibit the following relationship.

$$\frac{\Delta P}{L} = \frac{m}{k_1} U + \frac{d}{k_2} U^2 \qquad (4)$$

Flows exhibiting this relationship between pressure drop and velocity are known as non-Darcian flows. The two new terms, d and k_2, are, respectively, the fluid mass density and non-Darcian permeability. Once k_1 and k_2 are experimentally determined, there is an easy estimate of the filter's contribution to fluid flow.

2.1.6 Mold Permeability

One of the most important engineering considerations for aerospace sand castings is that there is sufficient ability for gasses to escape through the sand as metal is being poured. These pressurized gasses, which are being pushed out of the mold by the entering metal, are quite detrimental if not allowed to escape. On thin-walled castings, high backpressure in the mold cavity could possibly result in misruns. Also, core reaction defects begin to occur when gasses, generated by the breakdown of mold binder material, are not allowed to escape.

Considering the permeability of the sand mold material, eq. 3 can be used since gas escape velocities are quite low. By increasing the permeability of the sand, we can see that for a given required escape velocity, less of a pressure difference is required. This can be accomplished by compressing the sand less, producing a less dense, more porous structure. However, if the permeability of the sand is too high, molds will be considerably weaker than if they were tightly compressed. There is also the chance of having the molten metal penetrate the first few sand grain layers in the mold cavity, also known as metal burn-in. Depending on the amount of strength and permeability needed for a particular core, the engineer will select a composition of sand and binder that will

give the desired properties at a certain density. Besides the variation in sand/binder ratios inherent in industrial mixers and distributors, there is the added variation in density for any particular core produced in the foundry. This is mainly due to human variation and the fact that when humans perform an operation, it is never exactly the same twice. For this reason, any given core may vary in permeability throughout the material and from core to core. This range of possible permeability is different from foundry to foundry, machine to machine, and operator to operator. Simply using default permeability values for a generic type of sand/binder material may not be adequate. Values specific to the foundry may need to be determined to ensure accurate flow results.

2.2 Boundary Conditions

2.2.1 Wall Friction Factor

In order to allow the user better control over the physics of a simulation, the MAGMASOFT® code allows the wall friction boundary condition to be changed. This comes in the form of a friction factor, where a friction factor of 0.0 sets a free-slip flow boundary condition and a friction factor of 1.0 sets a no-slip flow boundary condition at the mold wall. The default setting is 0.0. This is because with most geometry having curved, non-rectangular surfaces, the jaggedness of the mesh as a result of curved geometry serves as an “artificial” wall friction. This is a result of the MAGMASOFT® mesh geometry, but when long flat walls exist, wall friction must be turned on. In reality, flow velocities are equal or close to zero, indicating that a more realistic model will incorporate the no-slip flow condition at mold walls. For flow through a relatively open, bulky cavity, the free-slip assumption is fine, but as casting wall thicknesses become smaller, velocity

profile produced with a no-slip boundary condition is critical. The question is, is this friction factor important for simulating a thin-walled aerospace casting?

2.2.2 Pouring Temperature

In the MAGMASOFT® casting simulation, the inlet pouring temperature is set as a constant boundary condition for all time during the pour. In reality, this temperature is a function of time and is really a result of the control of the melt temperature and the techniques used to get the metal from the melting furnace into the mold. In any casting process, it is critical to have knowledge of the inlet temperature condition throughout the pour within a reasonable tolerance when designing a mold. With this type of process, mold designs should be robust enough that they can accommodate pour temperatures in the range of +/-10 degrees of the specified pour temperature. For instance, if the design is robust enough to handle a pour temperature that is 10 degrees below the desired pour temperature, simulation results should indicate that the casting is problem-free. The trick is to be able to predict what this range will be in reality and design the appropriate gating and risering systems.

Using simulation as a design tool to cover the pour temperature variation is also dependent on the required casting quality and geometry. For example, if the casting does not have stringent requirements for inclusions resulting from filling turbulence and pores resulting from shrinkage and gas absorption, then the simulation accuracy is not as critical and it may only be necessary to see results at one mean pour temperature. However, greater required casting quality requires greater simulation accuracy for design, and possibly greater mold design robustness. Similarly, a more complex casting geometry often carries with it greater sensitivity to the pouring temperature variation. In this case,

more specific knowledge of the inlet pour temperature condition is required and it may be necessary to do a simulation at the extremes of the allowable casting tolerance to really see what happens when a casting is poured at the high temperature and low temperature extremes. If the pour temperature tolerance has a predictable effect on certain results on certain types of castings, it may not be necessary to do a simulation at the high and low values for similar castings in the future. Or conversely, the pour temperature tolerance could be increased allowing the pour-off department more liberty in making castings.

2.2.3 Metal Flow Rate

In an aerospace sand casting process, the metal flow rate is controlled by the size of the sprue choke and the metallostatic head pressure in the sprue and pouring basin. Since this process is almost exclusively human controlled, there is always a slight variation in the metal flow rate from one mold fill to another. This is quite noticeable in thin walled castings where a low head pressure in the pouring cup increases the casting susceptibility to misruns, while a high pouring cup head pressure increases the casting susceptibility to oxide film inclusions. It is desirable to produce mold designs robust enough to win the battle between preventing misruns and dross inclusions. It is also desirable to simulate pours at high and low values for the head pressure to examine a mold's robustness.

MAGMASOFT® allows the user to set the head pressure, total fill time or pouring rate at the inlet as a boundary condition for metal flow into the cavity. Since the real process utilizes control of the height of metal in the pouring cup to control the flow rate, a more realistic and advantageous approach would be to use the head pressure boundary condition. An idea of the variation in head pressure can be obtained through observing

the process. This behavior is different for different mold sizes, pouring techniques, and personnel performing the pour.

2.3 Summary

In the above sections, critical physical parameters have been discussed that outline requirements for obtaining successful simulation results. Since all results originate from the numerical calculation of coupled heat transfer and fluid flow equations, it is important to have correct values for the most influential parameters which are inputs to the model. Accordingly, the first step is to determine which parameters are the most influential and begin to quantify them first. This will give the best chance of obtaining accurate simulation results as early as possible in the development of a simulation tool. Five parameters, mold-metal heat transfer coefficient, mold thermal conductivity, wall friction factor, pouring basin head pressure, and pouring basin pouring temperature will be handled in the following sensitivity exercises to determine the most influential key parameters.

3. Sensitivity Analysis

3.1 Design of Experiments

The object of the sensitivity analysis was to consider thin walled aerospace sand castings and some corresponding defects commonly encountered in their development. By varying known key parameters that control the outcome of the casting process, the most influential parameters are identified and the importance of accurately determining certain quantitative database values is established. The first step is to start with a list of observable material defects, along with a list of corresponding mechanisms by which they are produced, and a list of the suspected key responsible parameters. The two defects identified below are critical in the design of thin walled structural aerospace sand castings and are the focus of this work.

Material Defect: Misrun	
Mechanism:	Metal becomes too cold and freezes before the cavity is completely filled. Heat transfer is too high, head pressure is too low. Surface tension of the oxide skin on the free surface may restrict flow. High back pressure.
Key Parameters:	Pour Temperature, mold-metal heat transfer coefficient, thermal conductivity of the mold, pouring cup height/fill time, filter permeability, metal free surface tension, mold permeability.

Material Defect: Dross/inclusions	
Mechanism:	Oxidation defects as a result of violent eddying of the melt flow. This behavior has been characterized to occur when average flow velocities are greater than 20in/sec. Also, when the metal front surface area of the melt becomes large, there is a greater chance of observing dross in the casting.
Key Parameters:	Height of pouring cup/fill time, wall friction factor

In this study, concentration was put on the misrun defect prediction. The reason for this is that misruns are one of the fundamental problems in metal casting and are extremely difficult to overcome when producing thin-walled aerospace sand castings. It is also one of the biggest challenges for computational software to accurately predict coupled heat transfer and fluid flow problems.

For the misrun investigation, two test geometry configurations were chosen. They were the fluidity spiral, shown in Figure 2 and a flat plate, shown in Figure 3. The top sprue dimension in Figure 2 is 1”x1”, and the plate dimensions in Figure 3 are 9”x21”x0.125” for reference.

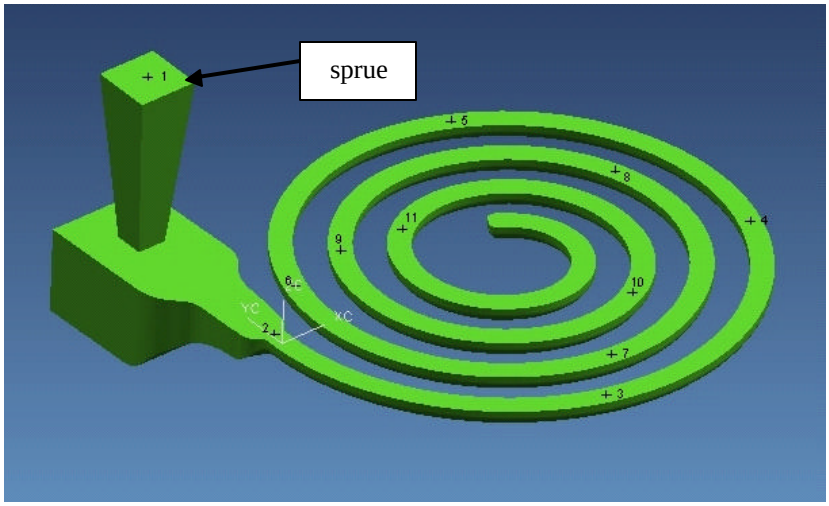

Figure 2: Fluidity Spiral and Temperature History Locations

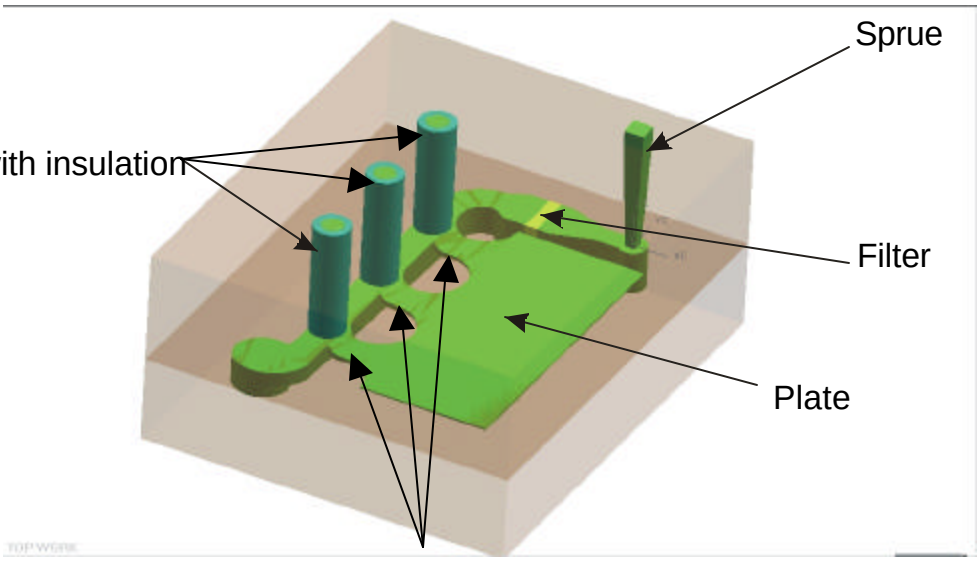

Figure 3: Thin Plate Geometry

All simulations were carried out using MAGMASOFT® casting simulation software. As this is a finite volume software package, all computations were carried out on a rectangular grid (Figure 4).

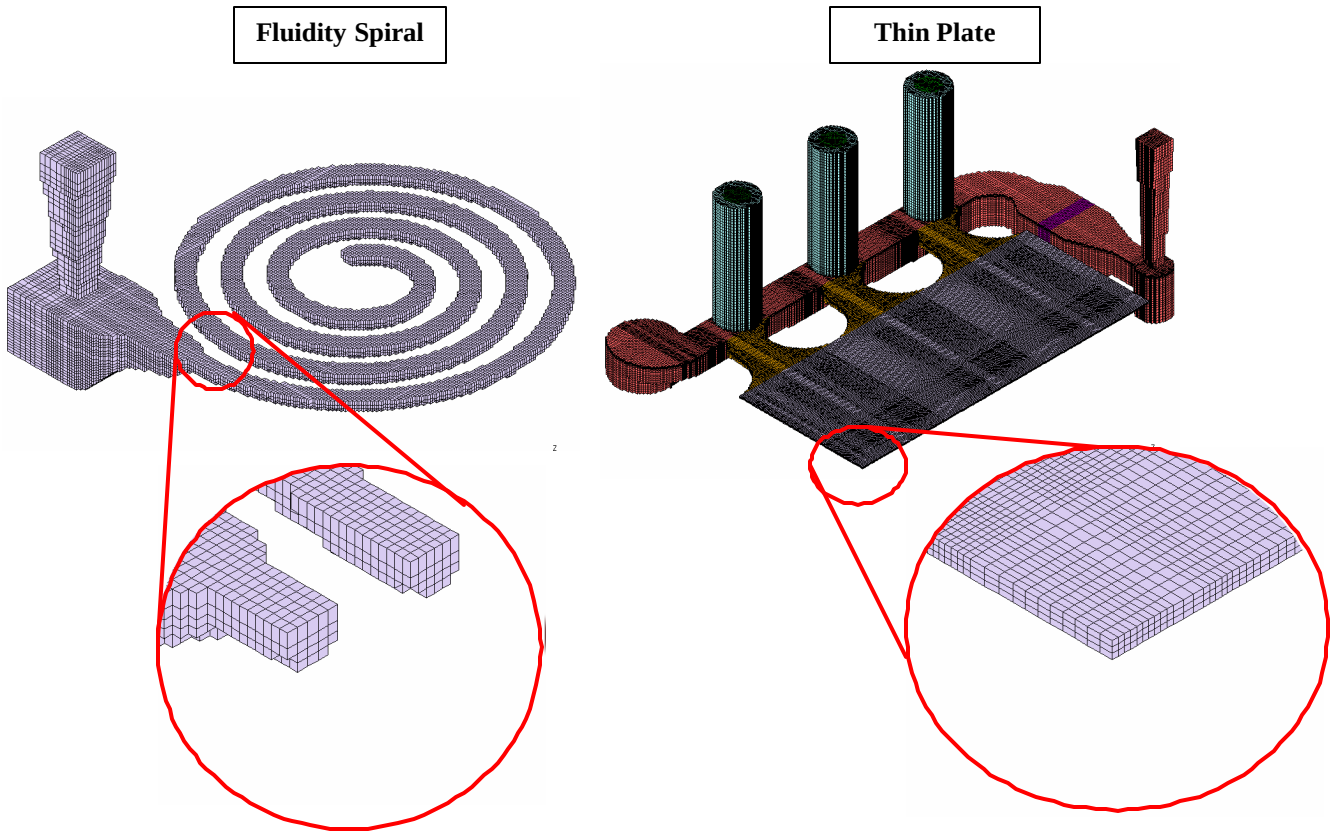

Figure 4: Mesh Geometry for Thin Plate and Fluidity Spiral

The mesh was constructed to allow for the fastest yet most accurate solutions possible. For the spiral, a sufficient amount of control volumes were placed across the spiral cross-section to allow for a good flow velocity profile, as is shown in Figure 4. This generated a mesh of 1,123,200 control volumes. For the thin plate, three control volumes were placed across the thin 0.125" dimension in the plate region. This generated a total mesh number of 11,462,256 control volumes. See Appendix A1 for more mesh parameters.

Subsequently, there was a need to establish a nominal set of casting parameters to work with. For the misrun sensitivity, all material parameters, such as alloy, mold, and interface thermophysical properties were set to the nominal values as existed in the database that most closely matched typical conditions in an aluminum aerospace casting

foundry. The alloy used for this study was the nominal 357 aluminum alloy existing in the MAGMASOFT® default database (AlSi7Mg06). The mold material was a chemically bonded urethane molding sand, with an AFS GFN of 50. See section 3.3 with more discussion on mold material properties. Appendix A1 shows additional pertinent simulation parameters for this nominal condition. The key parameters selected for consideration in this sensitivity analysis of a thin walled misrun defect were mold-metal heat transfer coefficient (HTC), sand thermal conductivity, wall friction factor, pour temperature, and metallostatic head pressure in the pouring basin.

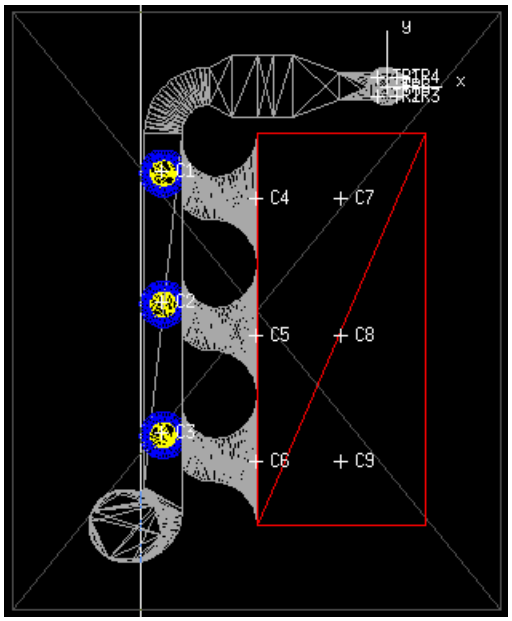

Figure 5: Temperature History Locations in Thin Plate

There are two types of results produced in this investigation. The first is temperature and velocity field results. Temperature and/or velocity fields are shown with colors representing metal temperatures and/or velocities in the cavity. A snapshot of the temperature field during the filling of the casting at a certain point in time is compared when the key parameter is varied and is a basis for comparison for sensitivity to heat transfer. Comparing the velocity fields shows the sensitivity of flow to a particular key

parameter. The second type of result is temperature history in curves at specified regions in the casting. These curves are generated, and when the parameter is varied, they are a basis of comparison for sensitivity to heat transfer. Temperature history locations for the fluidity spiral are found in Figure 2. Temperature history locations for the thin plate are found in Figure 5.

Method of Sensitivity Measurement

The sensitivity to variations in the key parameters will be measured three different ways. The first way to gauge the sensitivity of various key parameters to monitor at what point flow stopped in the fluidity spiral. A remarkable difference in the amount of fill from one value to another says that parameter is influential in the misrun phenomena. The second way the sensitivity of fill temperature to the various key parameters was gauged was by observing temperature-related quantities since most results are directly related to temperature results. A good candidate is the temperature loss from the inlet to a particular casting location, ΔT. This is a very practical quantity because it relates the inlet temperature, which is a controllable quantity, to the temperature at any particular point and time in the casting. If a pronounced variation is seen in the value of ΔT at any point with any change in a key parameter, then the conclusion would be that that key parameter is influential in the heat transfer during filling and subsequent solidification. This value will be examined for both the fluidity spiral geometry and the thin plate. The third way to practically assess the sensitivity is to consider a more localized portion casting geometry, such as the temperature loss, ΔT^* between two points close together. The temperature loss, ΔT^*, between these two points is critical for the filling of thin-walled geometry. It is possible to quantify how critical this value is by taking the ratio, $\frac{\Delta T^*}{\Delta T}$. The percentage of

the total temperature loss from the inlet occurring in the thin-walled region is quantified. Practically speaking, it may be necessary to add gates to ensure that the region fills before any misrun occurs if this ratio is too large. For this sensitivity analysis the ΔT^* considered is obtained from the thin plate geometry and is between points 4 (the closest ingate to the sprue) and 7 (plate region, closest to the sprue). The reason for these two points is that we have predetermined that the metal that passes through that gate also passes over the particular point in the plate.

3.2 Mold-Metal Heat Transfer Coefficient(HTC), h

Temperature Fields

The HTC was varied by adding or subtracting 50% of the nominal value. The reasoning for this particular choice of values is the fact that HTC have been observed in this range, and the recommended generic value of 1000 $W/(m^2K)$ is a good baseline for the sensitivity analysis. So the aim of this exercise is to examine the effects based on changes in the HTC within the practical ranges encountered in aerospace sand castings. Figure 6 shows slides of the temperature fields of the advancing melt in the fluidity spiral for three different constant mold-metal HTC values. There are two snapshots for each HTC value, one with the part 80% filled, and one after the

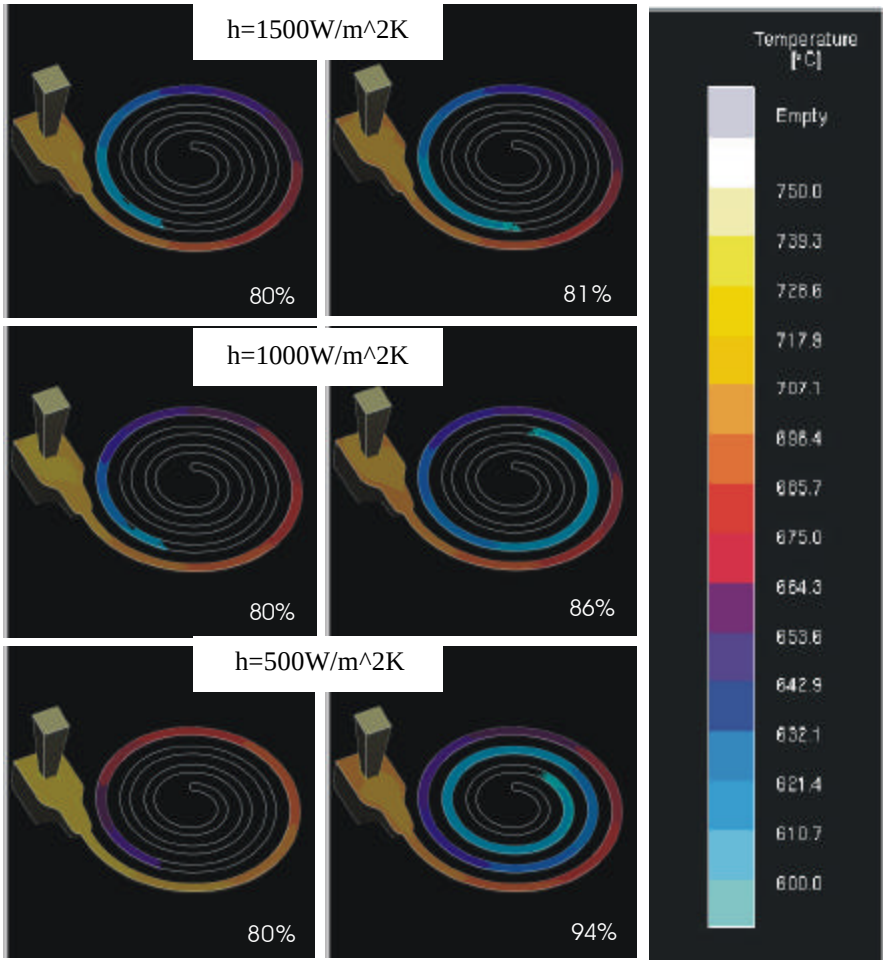

Figure 6: HTC Sensitivity Temperature Fields for Fluidity Spiral

front freezes, stopping the flow at 600°C. The scale is from the initial temperature of 750°C to the flow-stoppage temperature, set at 600°C. Upon examining the results, several issues become evident. The differences in the temperature fields at 80% filled give indications about how the heat transfer is affected by changing the HTC. The lighter blue colors shown with h=1500 indicate that heat transfer is occurring more rapidly than for the h=1000 or h=500 case. Another piece of information is the percentage of metal fills the cavity before it freezes. The fact that the metal stops flowing when it reaches a certain temperature illustrates the coupled energy and momentum transfer equations. A h=500 value allows the casting to fill 94%, while a h=1500 value allows the casting to fill only

81%. Notice that lowering the HTC changes the temperature field more drastically than increasing the HTC. This could be due to latent heat being expelled as metal begins to solidify in the mushy zone.

Figure 7 shows temperature fields for the thin plate. The scale extends from the solidus temperature, 534°C to the inlet temperature of 750°C. There was no flow stoppage temperature set for the thin plate geometry, so the casting will flow regardless of temperature. Notice how the thermal fields differ in the thin plate. Higher HTC values show an overall cooler temperature field, while lower HTC values show a higher overall temperature field. The rheological behavior also differs in the thin plate, and is evident in the slight variation in flow pattern. This shows the coupling between the solution to the momentum and energy equations. This is most likely due to the variation in density with temperature, as the code does not account for variation in viscosity with temperature or shear rate. For the thin plate, h=500 $W/(m^2K)$ produces a temperature field almost entirely above the liquidus while the nominal and high HTC produces a temperature field almost entirely in the mushy zone. Similar to the spiral, lowering the HTC seems to have more of an effect than raising the HTC. The shape of the temperature fields has changed due to the altered flow. Also, the initial splatter of metal in the furthest ingate from the sprue is more pronounced for the low and nominal HTC cases. It is not apparent why this is the case because the code does not account for surface tension effects and wall friction has been turned off.

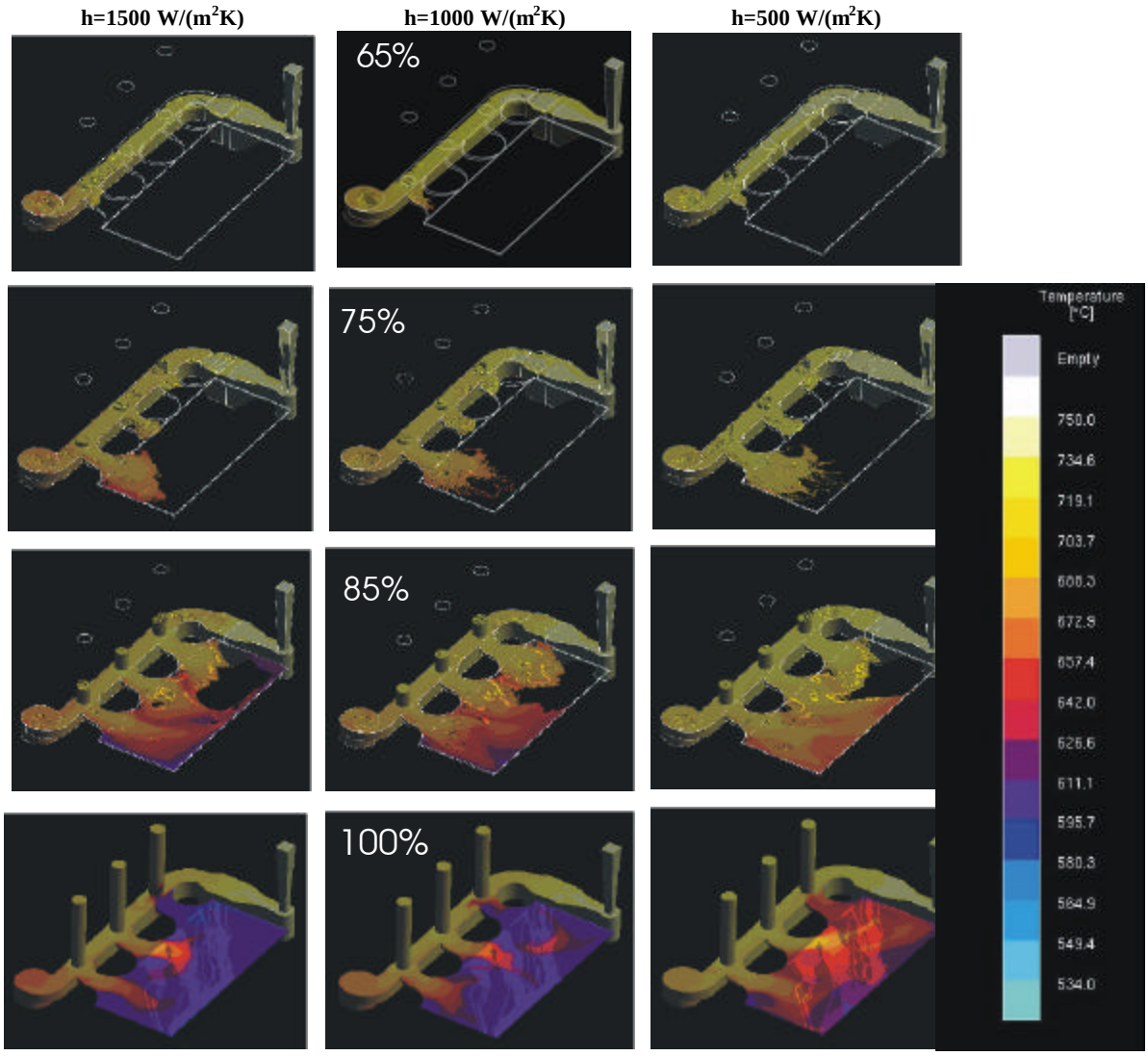

Figure 7: HTC Sensitivity Temperature Fields for Thin Plate

Cooling Curves

A graph of cooling curves at locations 2, 4, and 6 in the fluidity spiral is shown in Figure 8. Probe location 2 corresponds to the start, or 0%, along the spiral length. Probe location 4 corresponds to 20% along the spiral length. Probe location 6 corresponds to 40% along the spiral length.

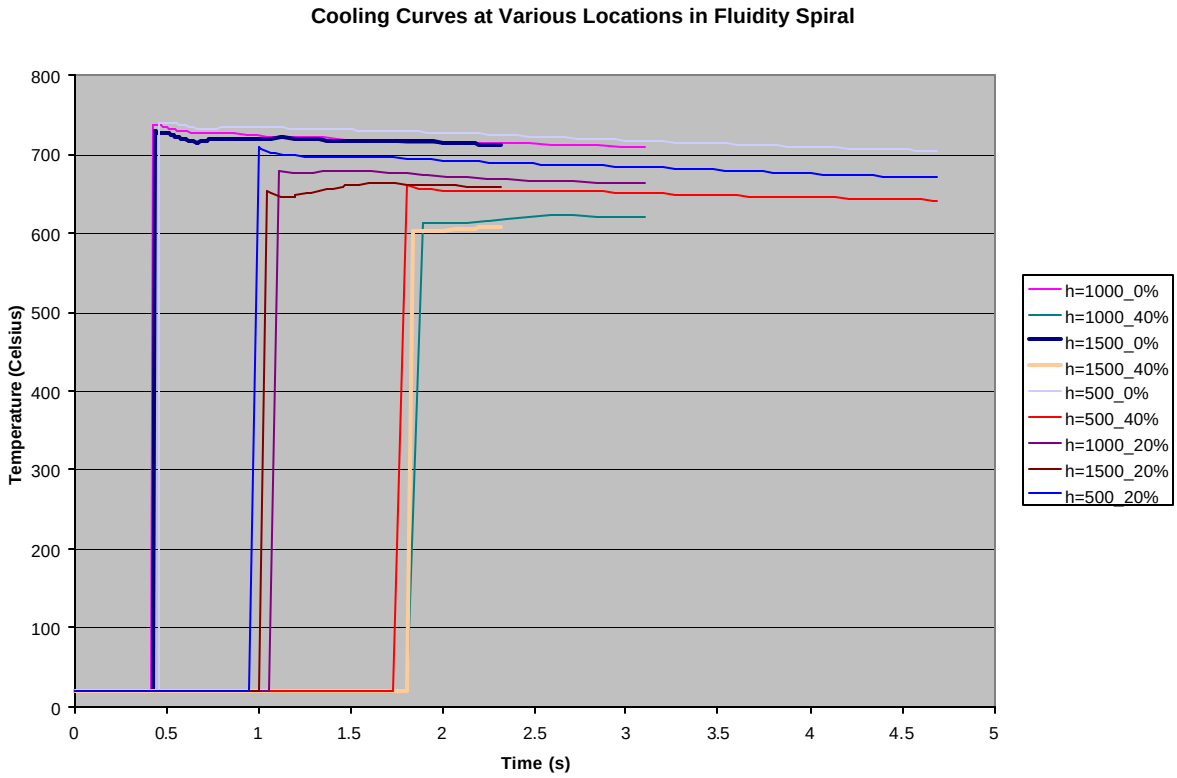

Figure 8: HTC Sensitivity Cooling Curves for Fluidity Spiral

Graphs of cooling curves in the plate, ingate, and riser portion of the thin plate casting are shown in Figure 9. Upon examining the temperature field pictures and cooling curve plots, several things are apparent. Upon examining Figure 7 and 9, it is easily seen that of the three probes in the plate region (Figure 5), the probe in the plate region furthest from the sprue (probe 9) registers first with the hottest metal in all cases. As time progresses, the temperature for each region decreases showing a certain cooling/heating rate. This is observed in the slope of the curves, dT/dt in Figure 9. The higher the cooling rate and the lower the initial temperature means the casting will solidify faster. Consequently, there is a greater possibility for misruns.

a. **Cooling Curves in Risers**

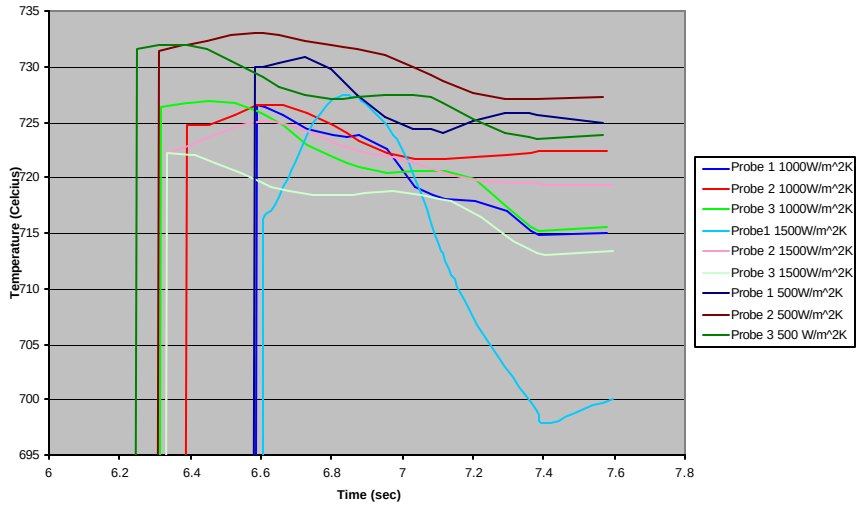

b. **Cooling Curves in Ingates**

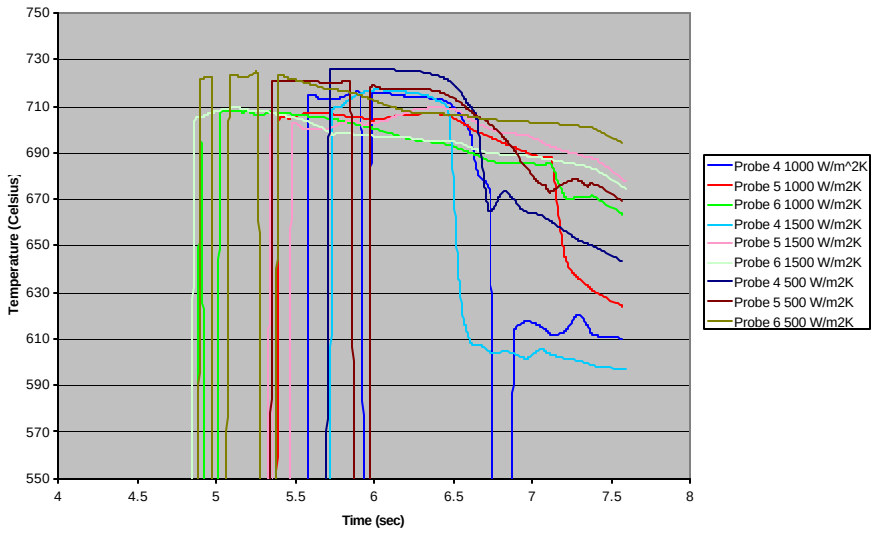

c. **Cooling Curves in Plate**

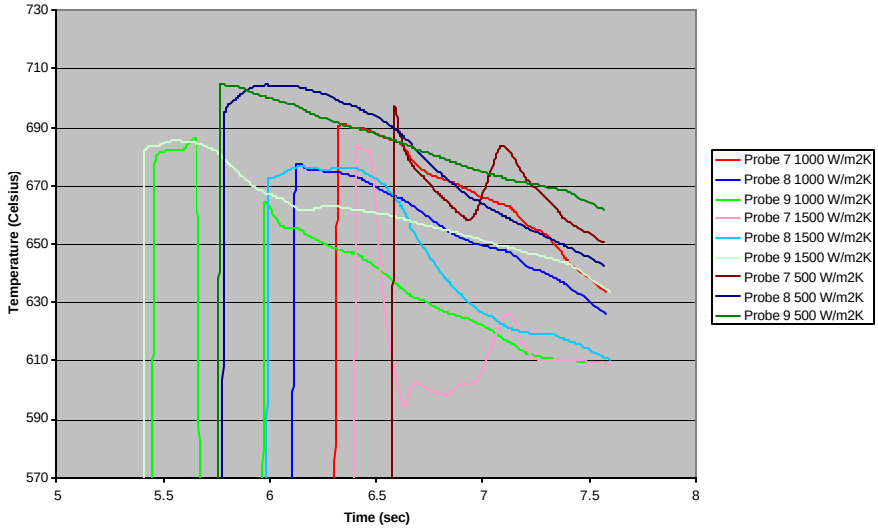

Figure 9: HTC Sensitivity Cooling Curves from Thin Plate

Clearly, the case with a high mold-metal HTC in Figure 7 shows the lowest plate temperatures throughout the fill. Also in the plate region, the low HTC value produces generally the lowest overall cooling rates. This is inferred from the shallow slope of the curves. The regions on the graph that appear to be discontinuous are simply a result of passing air pockets and flow convection. In the insulated risers, it would be expected that the cooling curves would be less sensitive to changes in HTC due to the higher Biot numbers encountered when heat is transferred through an interface into a relatively insulating mold.

Quantified Sensitivity Results

Upon computing ΔT values for the different probe locations for both the fluidity spiral and the thin plate, it is apparent that the system is sensitive to changing HTC values. Figure 10a and 10b shows

a. Metal Front Temperature Loss from Inlet to Probe # in Fluidity Spiral

	h=1500	h=1000	h=500
#4 $_{\Delta}$T	**96.78**	**71.60**	**41.70**
%difference	35.18%	----------	-41.76%
#6 $_{\Delta}$T	**146.38**	**139.27**	**89.84**
%difference	5.11%	----------	-35.49%

b. Casting Percentage Filled at Flow Stoppage

	h=1500	h=1000	h=500
% Filled	80.8	86.06	94.34
%difference	-6.11%	--------	9.62%

Figure 10: Quantified HTC Sensitivity Results for Fluidity Spiral

results for the fluidity spiral. Notice that the percent differences(yellow) in both ΔT and percent filled(green) are larger when the HTC is decreased than for when it is increased by the same amount.

Figure 11a,b, shows a summary of critical ΔT and ΔT^* values as well as averaged percent changes from the nominal conditions for the thin plate. Although the more

complex geometry of the plate produces more data, both scenarios support each other. In all cases, the system has a substantial percent difference in temperature loss when HTC is increased/decreased by 50%. It is also apparent that the further the metal travels, the larger the percent difference when the HTC deviates from the nominal value. The longest distance traveled would be that from the inlet to the plate probes and the average percent difference for the high and low HTC values are 3.92% and –23.53% respectively(yellow). The shortest distance traveled would be from the inlet to the ingate probes and those percent difference values are 3.68% and –38.24% for the respective high and low values. It is also apparent from Figure 11b that the heat loss in the thin-walled region is very significant compared to the rest of the geometry. If the ΔT^* value between probe 4 and 7 (closest ingate/plate probes to sprue) is considered for each of the three HTC values, this value is roughly 36%, 40%, and 54% of the total temperature loss, ΔT , from the inlet to probe 4 as the HTC is decreased(blue). This supports that the HTC in a thin-walled region is significant in this thin, flat section.

a. Metal Front Temperature Loss From Inlet to Probe				
		ΔT		
	Probe#	h=1500	h=1000	h=500
Risers	1	**34**	**23**	**20**
	% diff	47.83%	-----	-13.04%
	2	**28**	**25**	**19**
	% diff	12.00%	-----	-24.00%
	3	**28**	**24**	**19**
	% diff	16.67%	-----	-20.83%
Average		**30**	**24**	**19.33**
Avg % Difference		**25.00%**	**-----**	**-19.44%**
Ingates	4	**42**	**36**	**25**
	% diff	16.67%	-----	-30.56%
	5	**52**	**46**	**30**
	% diff	13.04%	-----	-34.78%
	6	**47**	**54**	**29**
	% diff	-12.96%	-----	-46.30%
Average		**47**	**45.33**	**28**
Avg % Difference		**3.68%**	**-----**	**-38.24%**
Plate	7	**66**	**60**	**54**
	% diff	10.00%	-----	-10.00%
	8	**78**	**73**	**57**
	% diff	6.85%	-----	-21.92%
	9	**68**	**71**	**45**
	% diff	-4.23%	-----	-36.62%
Average		**70.67**	**68**	**52**
Avg % Difference		**3.92%**	**-----**	**-23.53%**

b. Metal Front Temperature Loss From Ingate Probe 4 to Plate Probe 7			
ΔT* between Probe 7(ingate) and Probe 4(plate			
	h=1500	h=1000	h=500
	24	24	29
% difference	**0.00%**	**-----**	**20.83%**
% of DT	36.36%	40.00%	53.70%

Figure 11: Quantified HTC Sensitivity Results for Thin Plate

This percent difference means that if the nominal condition was taken to be the correct value, a diversion of 50% from this value will produce an error in temperature results that is the same as the percent differences in Figure 11. Also, it appears as though a decrease in mold-metal HTC has more of an affect on heat transfer than an increase by the same factor.

3.3. Mold Thermal Conductivity, λ

In general, it is the thermal conductivity of the mold material that restricts the majority heat transfer in sand castings due to the relatively high Biot numbers encountered, as discussed in section 2.1. This is more the case for bulkier, thicker wall-sectioned castings, and the thinner the wall sections become, the lower the Biot number becomes and the more the mold-metal HTC is competing with the mold thermal conductivity for heat flow control. For this reason, it is desirable to investigate the temperature sensitivity to the mold thermal conductivity for a thin-walled region.

The thermal conductivity primarily varies with temperature. For this analysis, values were taken at the upper extreme to be 1.5 times the nominal value at any particular temperature. The lower extreme was taken to be 0.5 times the nominal value. This is consistent with the +/-50% variation in the HTC in the previous section. It also is a very practical representation when varying materials in the foundry. Zircon sands have measured λ-values that come close to 1.5 times the nominal values. Experimentally measured thermal conductivity of chemically bonded urethane mold sand with silica grains having an AFS GFN#50 is typically described as a function of temperature and is shown below in Figure 12 [4].

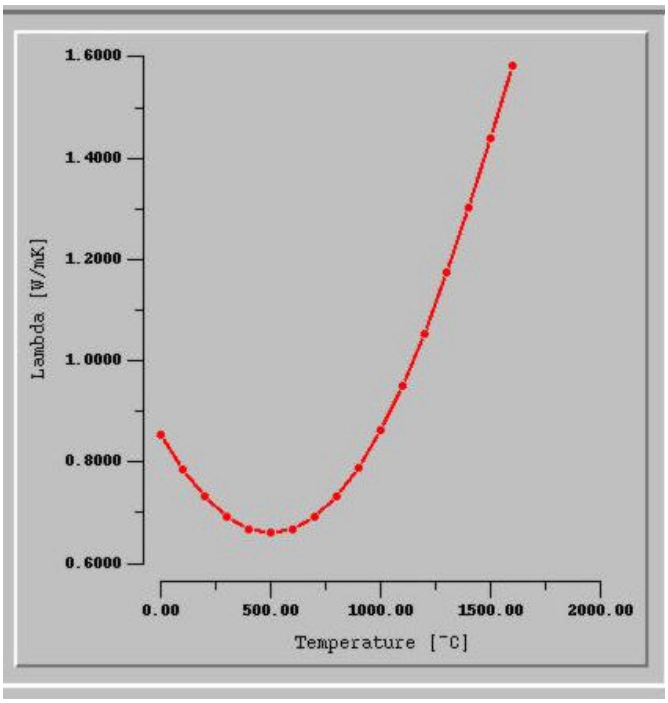

Figure 12: Nominal Mold Thermal Conductivity

The sensitivity to variations of λ is handled in the same way as for the mold-metal HTC.

Temperature Fields

Figure 13 shows temperature field results for the fluidity spiral for three different thermal conductivity data sets. Upon examining Figure 13, results look similar to those for the HTC sensitivity results. Upon increasing λ, there is a cooler overall temperature field and the metal fills the mold less than for a decrease in thermal conductivity. It can be clearly noted that a 50% change increase or decrease from the nominal value has less of an impact on the temperature field result than when the HTC is varied.

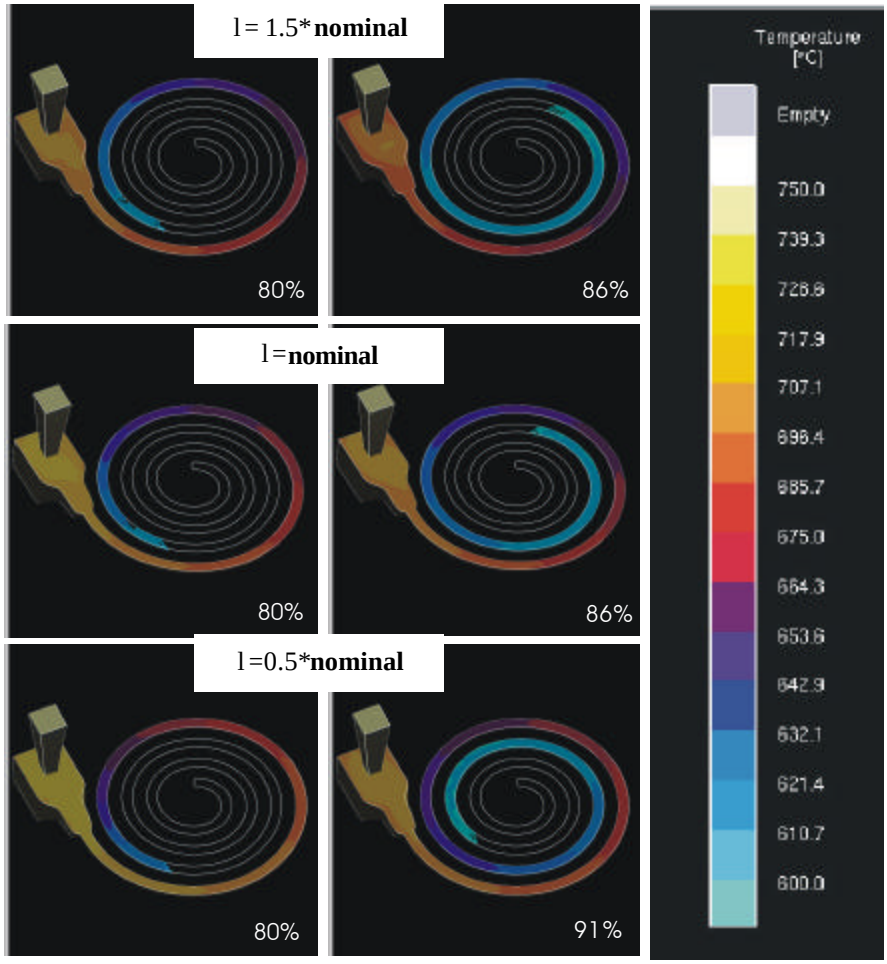

Figure 13: Thermal Conductivity Sensitivity Temperature Fields for Fluidity Spiral

Figure 14 shows temperature field results for the thin plate. Upon examining the above temperature fields, the results are similar to variations in the mold-metal HTC; however, there are subtle differences. Again this supports the Figure 6 and 7 results that a +/-50% change in HTC has more of an effect than a +/-50% change in λ.

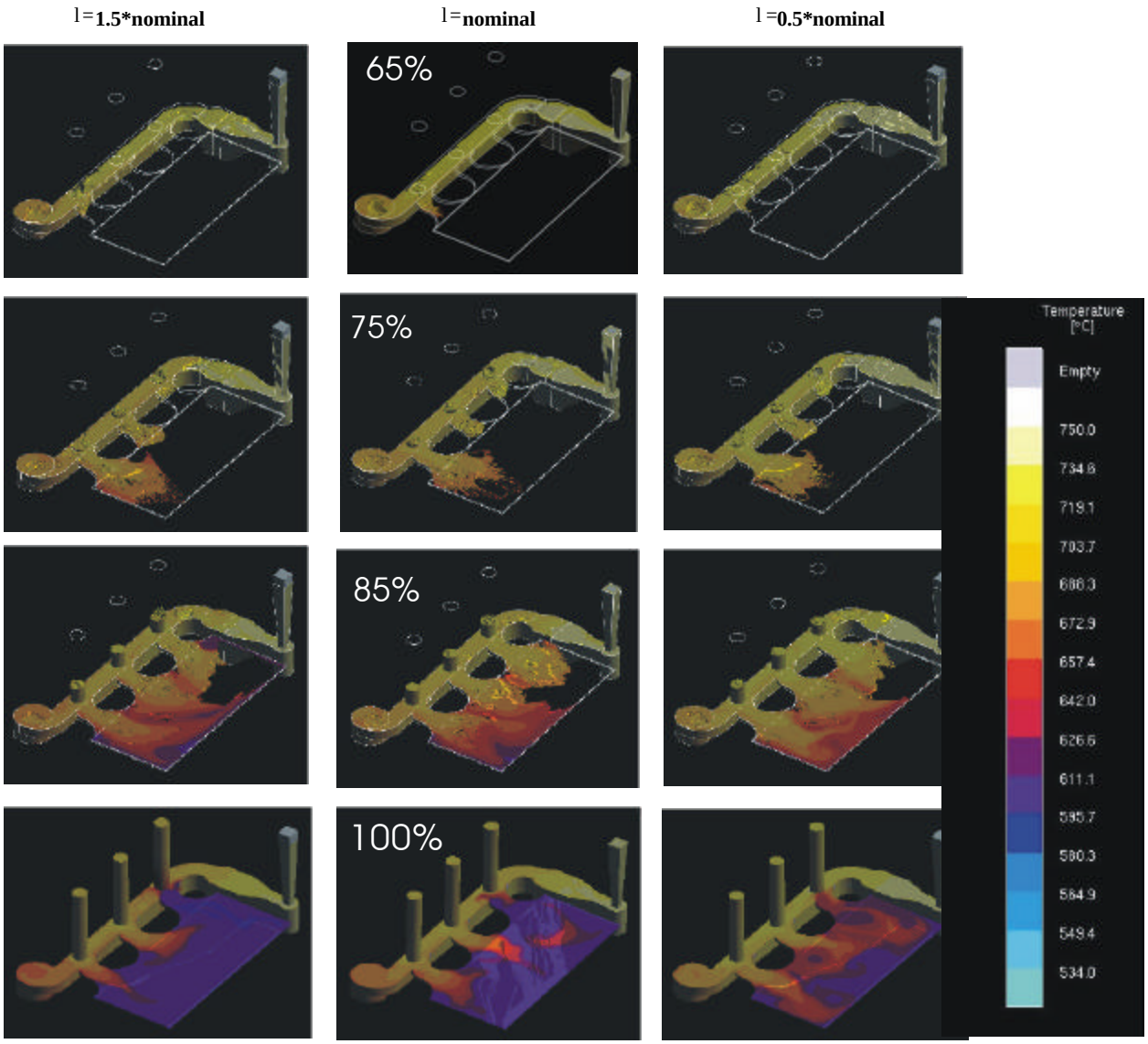

Figure 14: Mold Thermal Conductivity Sensitivity for Thin Plate

Cooling Curves

Cooling curves for varying the mold thermal conductivity can be found in Appendix A2.

Quantified Sensitivity Results

Figure 15a and 15b shows ΔT sensitivity to variation in the mold thermal conductivity for the fluidity spiral. Notice how the percent difference value for probe 4 with a 50% increase in mold thermal conductivity is 4.0%, while the percent difference with a

50% increase in HTC is 35.18%. The same observations exist for the rest of the data, indicating that a 50% increase or decrease in HTC is more influential in controlling heat transfer for short times and with thin-walled geometry.

Figure 16a and 16b shows similar results for the thin plate geometry. The portions of Figure 16 of concern are the areas in yellow. Using these measures, it is apparent that changing the mold thermal conductivity by this factor does have an effect on the mold's ability to transfer heat. The first thing to notice is that in the plate region, an increase in mold thermal conductivity shows a more pronounced temperature loss sensitivity than an equivalent decrease. This can be seen in the 12.75% and –7.35% difference (yellow) from the nominal condition. The second thing that can be seen is that the percentage of the total heat loss in the plate region (blue) deviates almost equally from the nominal value whether the thermal conductivity is equally increased or decreased.

a. Metal Front Temperature Loss from Inlet to Probe # in Fluidity Spiral				**b. Casting Percentage Filled at Flow Stoppage**			
	k=1.5*nom	k=nom	k=0.5*nom		k=1.5*nom	k=nom	k=0.5*nom
#4 ΔT	**74.46**	**71.56**	**60.94**	% Filled	85.75	86.06	90.54
%difference	4.00%	----------	-14.88%	%difference	-0.36%	--------	5.21%
#6 ΔT	**140.02**	**139.27**	**125.36**				
%difference	0.54%	----------	-9.99%				

Figure 15: Quantified Mold Thermal Conductivity Sensitivity Results for Fluidity Spiral

a. Metal Front Temperature Loss From Inlet to Probe

	Probe#	ΔT 1.5k	ΔT k	ΔT .5k
Risers	1	**27**	**23**	**20**
	% diff	17.39%	-----	-13.04%
	2	**26**	**25**	**19**
	% diff	4.00%	-----	-24.00%
	3	**27**	**24**	**21**
	% diff	12.50%	-----	-12.50%
Average		**26.67**	**24**	**20**
Avg % Difference		**11.11%**	-----	**-16.67%**
ngates	4	**43**	**36**	**30**
	% diff	19.44%	-----	-16.67%
	5	**53**	**46**	**34**
	% diff	15.22%	-----	-26.09%
	6	**45**	**54**	**35**
	% diff	-16.67%	-----	-35.19%
Average		**47**	**45.33**	**33**
Avg % Difference		**3.68%**	-----	**-27.21%**
Plate	7	**82**	**60**	**57**
	% diff	36.67%	-----	-5.00%
	8	**75**	**73**	**69**
	% diff	2.74%	-----	-5.48%
	9	**73**	**71**	**63**
	% diff	2.82%	-----	-11.27%
Average		**76.67**	**68**	**63**
Avg % Difference		**12.75%**	-----	**-7.35%**

b. Metal Front Temperature Loss From Ingate Probe 4 to Plate Probe 7

ΔT* between Probe 7(ingate) and Probe 4(plate)	1.5k	k	.5k
	39	24	27
% difference	**62.50%**	-----	**12.50%**
% of DT	47.56%	40.00%	47.37%

Figure 16: Quantified Thermal Conductivity Sensitivity Results for Thin Plate

3.4 Wall Friction Factor

It is desirable to see the effects of turning on and off wall friction for casting geometry that has flat, straight walls and one that has curved walls. The flat walls will show how wall friction affects results with a smooth, straight mesh. The curved walls in the spiral will show how wall friction affects results with a jagged mesh

Temperature and Velocity Fields

Figure 17 shows slides of the advancing melt with the temperature fields for the thin plate. Upon comparing the two results, it is readily qualitatively apparent that wall friction has a huge impact on the metal flow

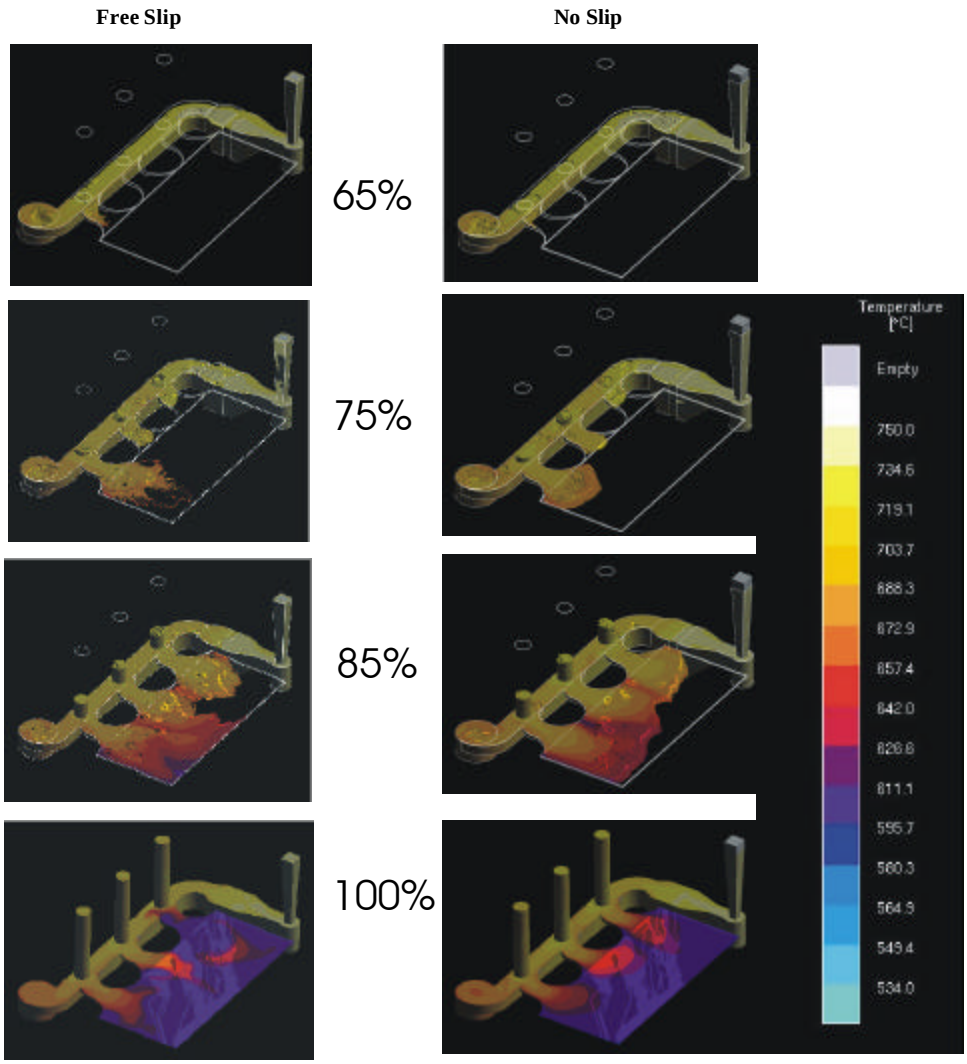

Figure 17: Friction Factor Sensitivity Temperature Fields for Thin Plate

profile, especially in the plate region. Also, the temperature fields look similar in the runner, but when metal enters the plate, the results differ. This shows the coupling between flow and heat transfer, whereby changing strictly a flow parameter has a direct effect on temperature results of the system. Figure 18 shows the dynamic effects of changing wall friction showing melt velocity fields of the thin plate. At 65% filled, there is no major difference in local velocity in any region of the gating. Once the metal enters the plate, there is a drastic difference. Metal with the free slip boundary condition appears to

splatter into the plate, whereas metal in the no slip condition has a very quiescent flow. The no slip condition clearly shows a more realistic flow for the flat geometry than the free slip condition.

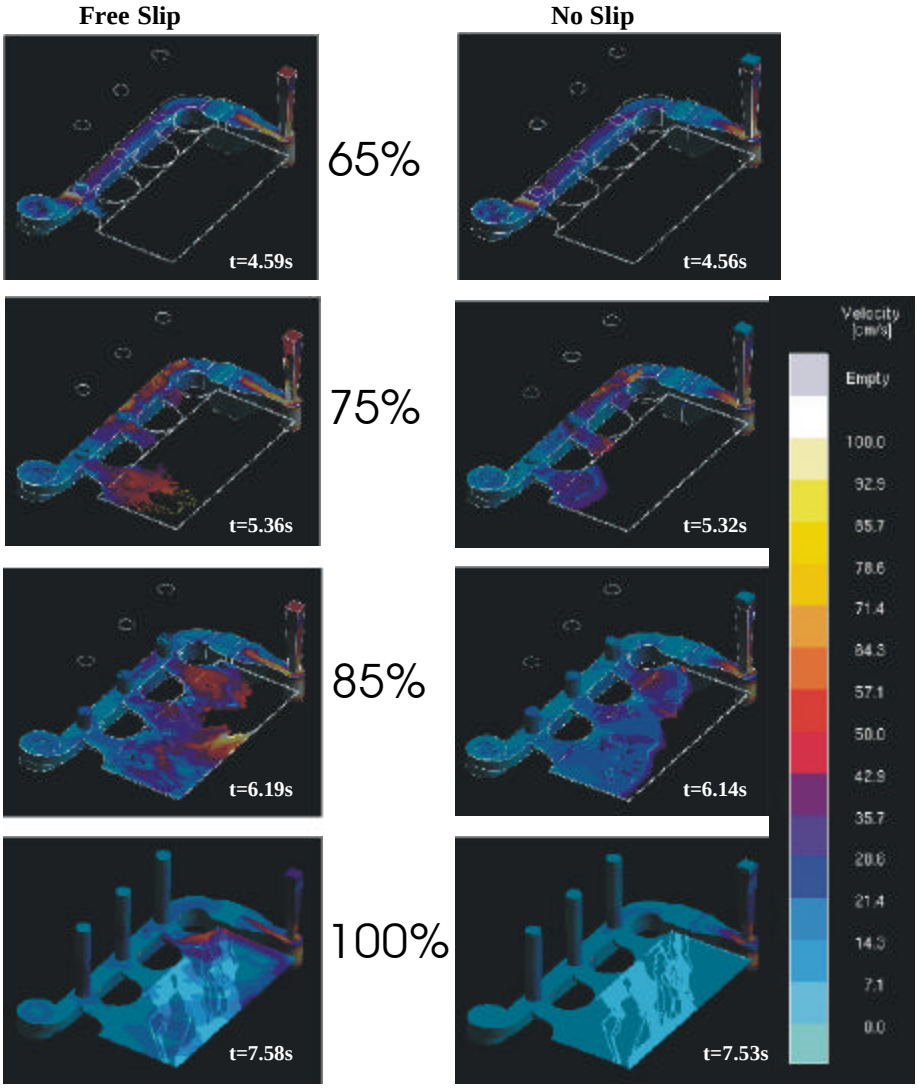

Figure 18: Friction Factor Sensitivity Velocity Fields for Thin Plate

The fluidity spiral geometry is not as responsive to changes in the wall friction boundary condition. Since there are no long, flat regions, the jagged mesh reduces the velocities at the mold wall enough to effectively provide a wall resistance. Figure 19 shows the negligible diffenence in both the temperature field and final fill percentage.

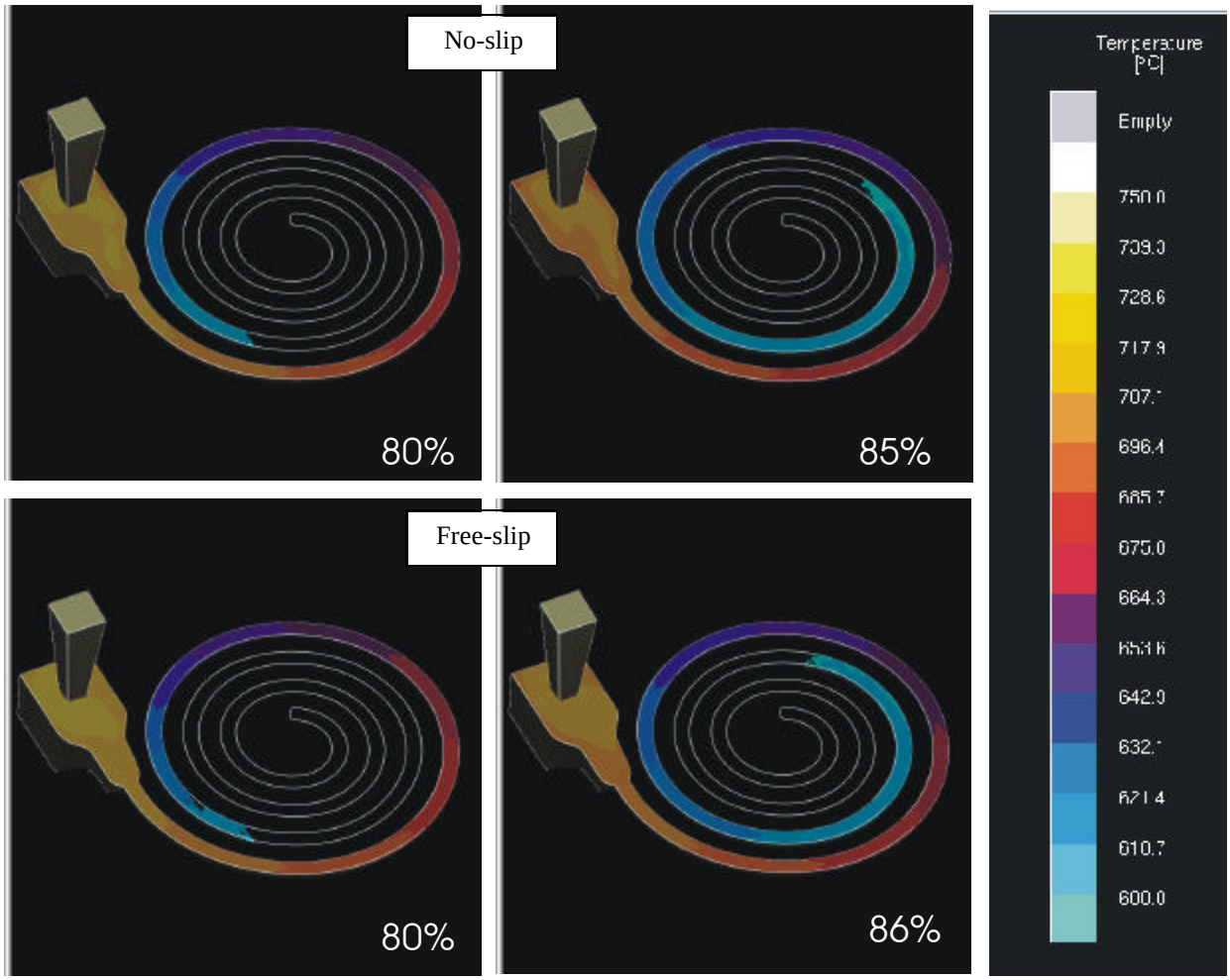

Figure 19: Friction Factor Sensitivity Temperature Fields for Fluidity Spiral

Cooling Curves

Cooling curves for the slip and no-slip boundary condition are found in Appendix A3.

Quantified Sensitivity Results

Figure 20 shows the change in temperature loss between a no slip and free slip boundary conditions as well as the percent difference in fill percentage for the fluidity spiral. Notice how the highlighted numbers in Figure 20 are similar to those in Figure 15.

a. Metal Front Temperature Loss from Inlet to Probe # in Fluidity Spiral			b. Casting Percentage Filled at Flow Stoppage		
	no-slip	free-slip		no-slip	free-slip
#4 ΔT	**74.81**	**71.59**	% Filled	85.23	86.06
%difference	4.49%	----------	%difference	-0.96%	--------
#6 ΔT	**141.81**	**139.27**			
%difference	1.83%	----------			

Figure 20: Quantified Friction Factor Sensitivity Results for Fluidity Spiral

Figure 21 shows temperature loss data for the thin plate. Notice how there is virtually no difference between the no-slip and free-slip condition in this figure.

a. Metal Front Temperature Loss From Inlet to Probe				b. Metal Front Temperature Loss From Ingate Probe 4 to Plate Probe 7		
	Probe#	ΔT		ΔT* between Probe 7(ingate) and Probe 4(plate)		
		no-slip	free-slip		h=1500	h=1000
Risers	1	**23.47**	**23**		24.33	24
	% diff	2.05%	-----	**% difference**	**1.38%**	**-----**
	2	**25.39**	**25**	**% of DT**	40.44%	40.00%
	% diff	1.55%	-----			
	3	**23.77**	**24**			
	% diff	-0.97%	-----			
Average		**24.21**	**24**			
Avg % Difference		**0.87%**	**-----**			
Ingates	4	**35.83**	**36**			
	% diff	-0.46%	-----			
	5	**45.90**	**46**			
	% diff	-0.22%	-----			
	6	**54.22**	**54**			
	% diff	0.40%	-----			
Average		**45.32**	**45.33**			
Avg % Difference		**-0.04%**	**-----**			
Plate	7	**60.17**	**60**			
	% diff	0.28%	-----			
	8	**73.29**	**73**			
	% diff	0.40%	-----			
	9	**71.10**	**71**			
	% diff	0.15%	-----			
Average		**68.19**	**68**			
Avg % Difference		**0.28%**	**-----**			

Figure 21: Quantified Friction Factor Sensitivity Results for Thin Plate

It appears as though there is a big influence of the wall friction and resultant flow behavior of metal in thin walled regions where the wall is long and flat. This influence is such that geometry with long flat walls producing an alligned mesh would show more realistic results when the wall friction is turned on.

3.5 Pouring Temperature

One of the challenges in designing aerospace sand molds is to construct a mold that is robust enough to produce quality castings despite a ±10°C metal pouring temperature variation. Normally, simulations would need to be performed at both extremes of the process parameters to explore the robustness of the mold design. However, if this variation is explored for characteristic casting geometry, it may be possible to have a good idea of what the effects would be for a real casting by only conducting one simulation at nominal values. For this reason, it is desirable to see the effects of varying the pouring temperature of different casting geometry by ±10°C. In this study, the effects on a thin-walled aluminum sand casting will be shown and this sort of analysis can be carried over to different types of geometry such as wall junctions, bosses and pads, and internal passage walls.

Temperature Fields

Figure 22 shows temperature field results for three values of inlet (sprue) pouring temperatures for the spiral geometry. The high and low values of T=760°C and T=740°C correspond to the ±10°C temperature variation that is expected in the foundry. Notice that there is not much qualitative difference in percentage filled between the high and low pouring temperature conditions—all the simulations fill essentially the same.

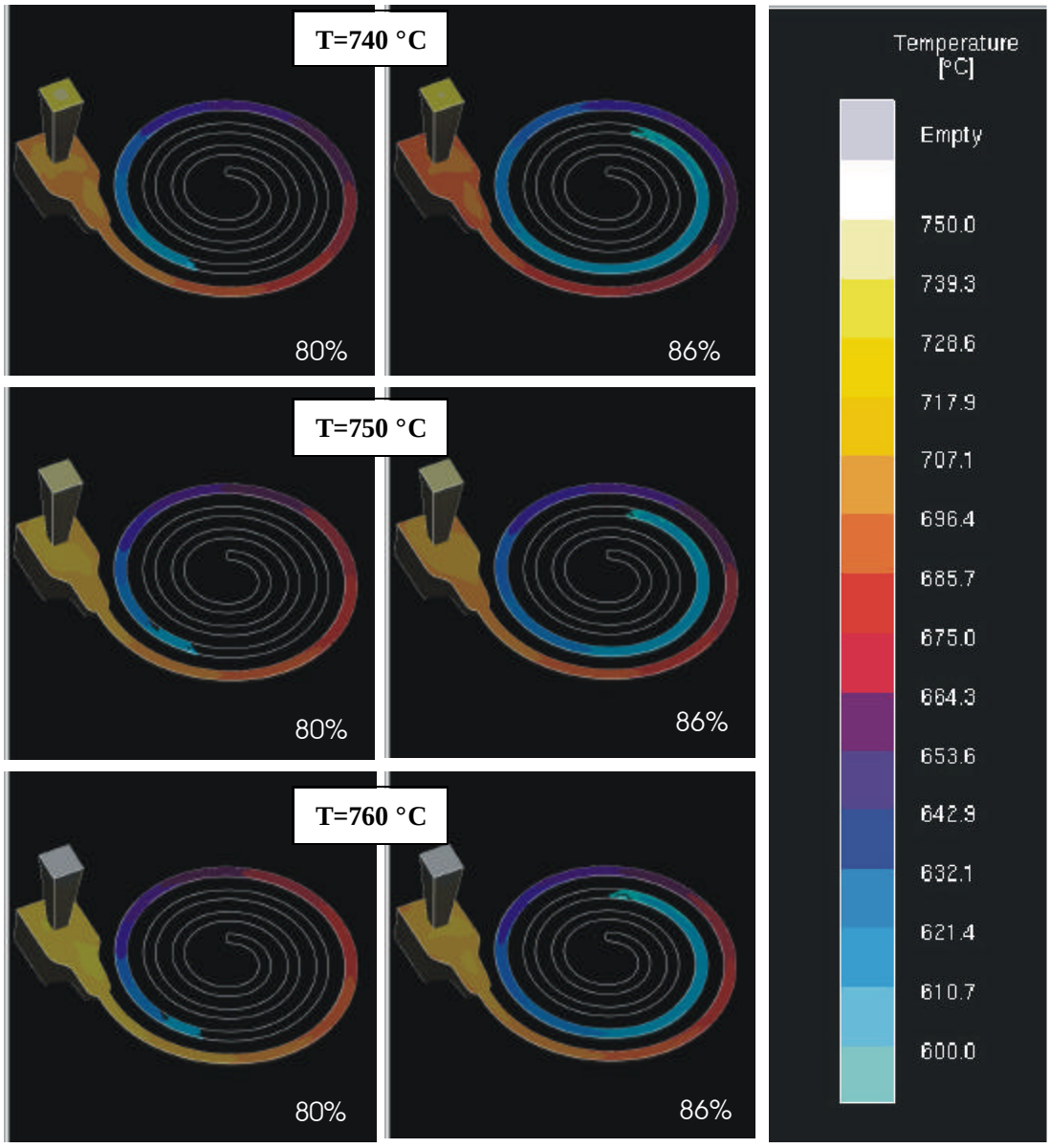

Figure 22: Pour Temperature Sensitivity Temperature Fields for Fluidity Spiral

Figure 23 shows temperature field results for three values of inlet pouring temperature for the thin plate geometry.

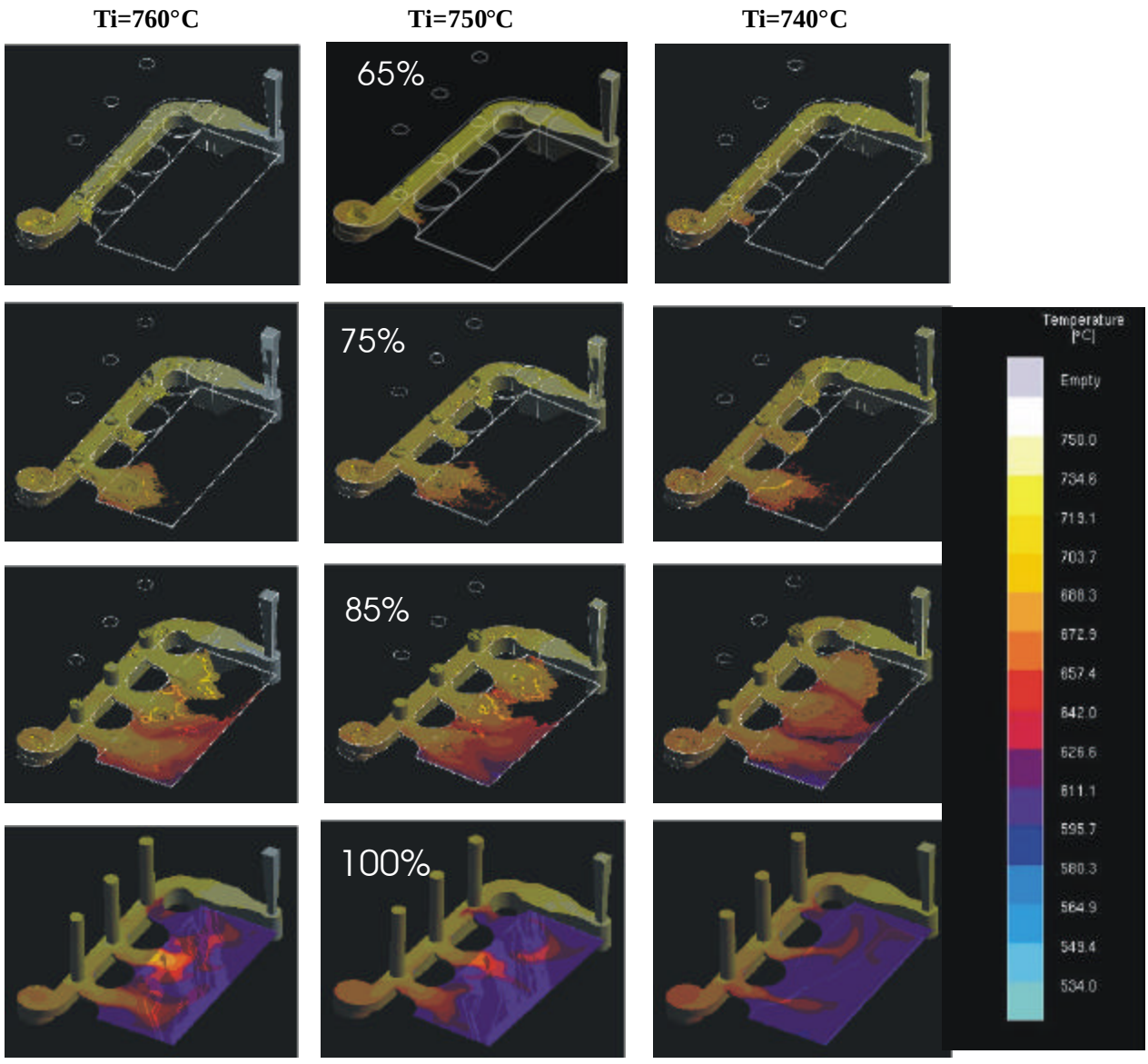

Figure 23: Pouring Temperature Sensitivity for Thin Plate

Upon examining Figure 23, the metal at the colder pouring temperature has a slightly cooler temperature field overall. A pour temperature of 760°C produces temperature field results that are slightly higher overall. Of course, subtle differences are noted in the contours of isotherms due to the coupling between fluid flow and heat transfer. The important information is in the trends and the general behavior of the metal as it fills the cavity.

Cooling Curves

Cooling curves for the three inlet pouring temperatures are shown in Appendix A4.

Quantified Sensitivity Results

a. Metal Front Temperature Loss from Inlet to Probe # in Fluidity Spiral				**b. Casting Percentage Filled at Flow Stoppage**			
	T=740°C	T=750°C	T=760°C		T=740°C	T=750°C	T=760°C
#4 ΔT	**73.18**	**71.60**	**72.89**	% Filled	86.27	86.06	86.08
%difference	2.21%	----------	1.80%	%difference	0.24%	--------	0.02%
#6 ΔT	**131.17**	**139.27**	**144.97**				
%difference	-5.82%	----------	4.10%				

Figure 24: Quantified Pouring Temperature Sensitivity Results for Fluidity Spiral

Figure 24 shows mixed results. It shows a corresponding lower temperature loss for a lower inlet pour temperature and a higher temperature loss for a higher inlet pour temperature at probe #6, but the opposite is true for probe #4. At probe #4, there is greater temperature loss than for the nominal condition in both cases. It should also be noted that in Figure 25, the yellow highlighted regions both show a decrease in temperature loss from the nominal condition. Again, it appears as though there is no correlation between inlet pour temperature and heat loss.

a. Metal Front Temperature Loss From Inlet to Probe

	Probe#	ΔT T=760	ΔT T=750	ΔT T=740
Risers	1	**28**	**23**	**27**
	% diff	21.74%	-----	17.39%
	2	**24**	**25**	**26**
	% diff	-4.00%	-----	4.00%
	3	**25**	**24**	**24**
	% diff	4.17%	-----	0.00%
Average		**25.67**	**24**	**25.67**
Avg % Difference		**6.94%**	-----	**6.94%**
Ingates	4	**35**	**36**	**33**
	% diff	-2.78%	-----	-8.33%
	5	**46**	**46**	**39**
	% diff	0.00%	-----	-15.22%
	6	**42**	**54**	**55**
	% diff	-22.22%	-----	1.85%
Average		**41**	**45.33**	**42.33**
Avg % Difference		**-9.56%**	-----	**-6.62%**
Plate	7	**55**	**60**	**54**
	% diff	-8.33%	-----	-10.00%
	8	**80**	**73**	**72**
	% diff	9.59%	-----	-1.37%
	9	**60**	**71**	**66**
	% diff	-15.49%	-----	-7.04%
Average		**65**	**68**	**64**
Avg % Difference		**-4.41%**	-----	**-5.88%**

b. Metal Front Temperature Loss From Ingate Probe 4 to Plate Probe 7

ΔT* between Probe 7(ingate) and Probe 4(plate)	T=760	T=750	T=740
	20	24	21
% difference	**16.67%**	-----	**12.50%**
% of DT	36.36%	40.00%	38.89%

Figure 25: Quantified Pouring Temperature Sensitivity Results for Thin Plate

3.6 Pouring Basin Head Pressure

In addition to the variation in pour temperature that is encountered with the sand casting process, there is the added variation in the way metal is poured into the pouring basin. This can have dramatic effects on the flow of metal into the mold and the resulting casting that is produced. Ideally, one would like to have the same pour every time, but since this is a human-controlled process, variation in ladle pours exist from operator to operator and even from mold to mold. Therefore it is important to have an idea of the range of possibilities for this part of the process, and especially the effect on characteristic thin-walled geometry. In this analysis, it was estimated that a typical pourer could produce a basin head height tolerance of ±1". Figure 26 shows the action of pulling the plug and arriving at an initial head pressure condition at the top of the sprue. Notice the first picture

shows the plug in the cup. At this point, the pressure is ambient. Immediately after the plug is pulled, the pressure increases as it fills the void the plug once occupied, and promptly arrives at an initial value. The pourer then continuously adds metal to the basin, maintaining a constant level to the best of his ability. Figure 27 shows the resultant head pressure vs. time curve that is imposed as a boundary condition at the top of the sprue and governs the filling of the cavities. These curves model the pouring basin plug being pulled and head pressure values at the top of the sprue coming to various head heights of 3", 4", and 5" respectively.

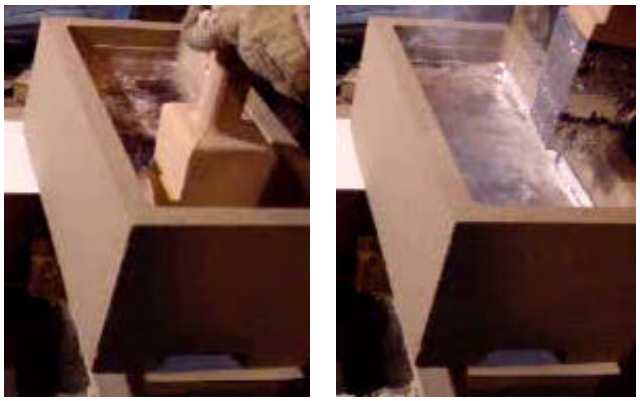

Figure 26: Plug Pull from Pouring Basin

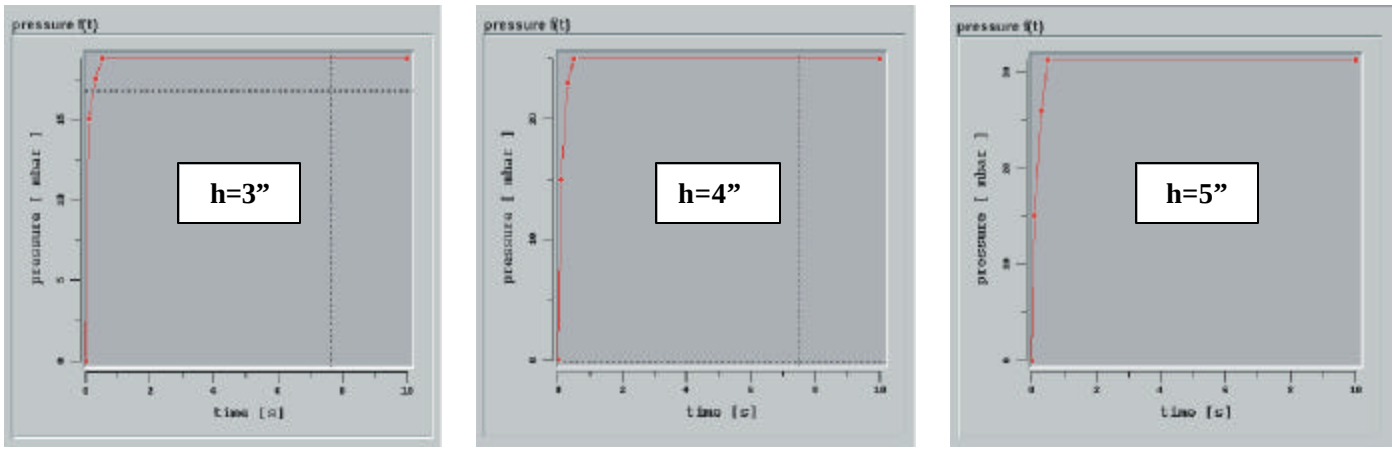

Figure 27: Pressure vs. Time Curves for Inlet Boundary Condition

Temperature Fields

The following temperature field results are in Figure 28 for the spiral and Figure 29 for the thin plate, showing a nominal head pressure of 4". In Figure 28, the spiral fills more with a higher head and less with a lower head. Differences in the isotherms are not easily noticed. This is also the case in Figure 29 of the plate. It is not until the end of the pour that slight differences are noticed, and this could be attributed to the dynamic effects of convection. The most noticeable difference is seen in the velocity fields of Figure 30, and specifically the time it takes for metal to fill certain portions in the mold. Notice how a higher head pressure decreases fill times by 3.5% to 4% while a lower head pressure increases fill times by 3.9% to 4.4%. In reality, these values could be the deciding factor on whether or not there will be a misrun in a thin walled casting. It is surprising that the h=3in run doesn't have a lower overall temperature field due to the extra time heat is allowed to escape into the mold. The time delay of 4% must not be great enough to allow much more heat to escape, even in this thin-walled section.

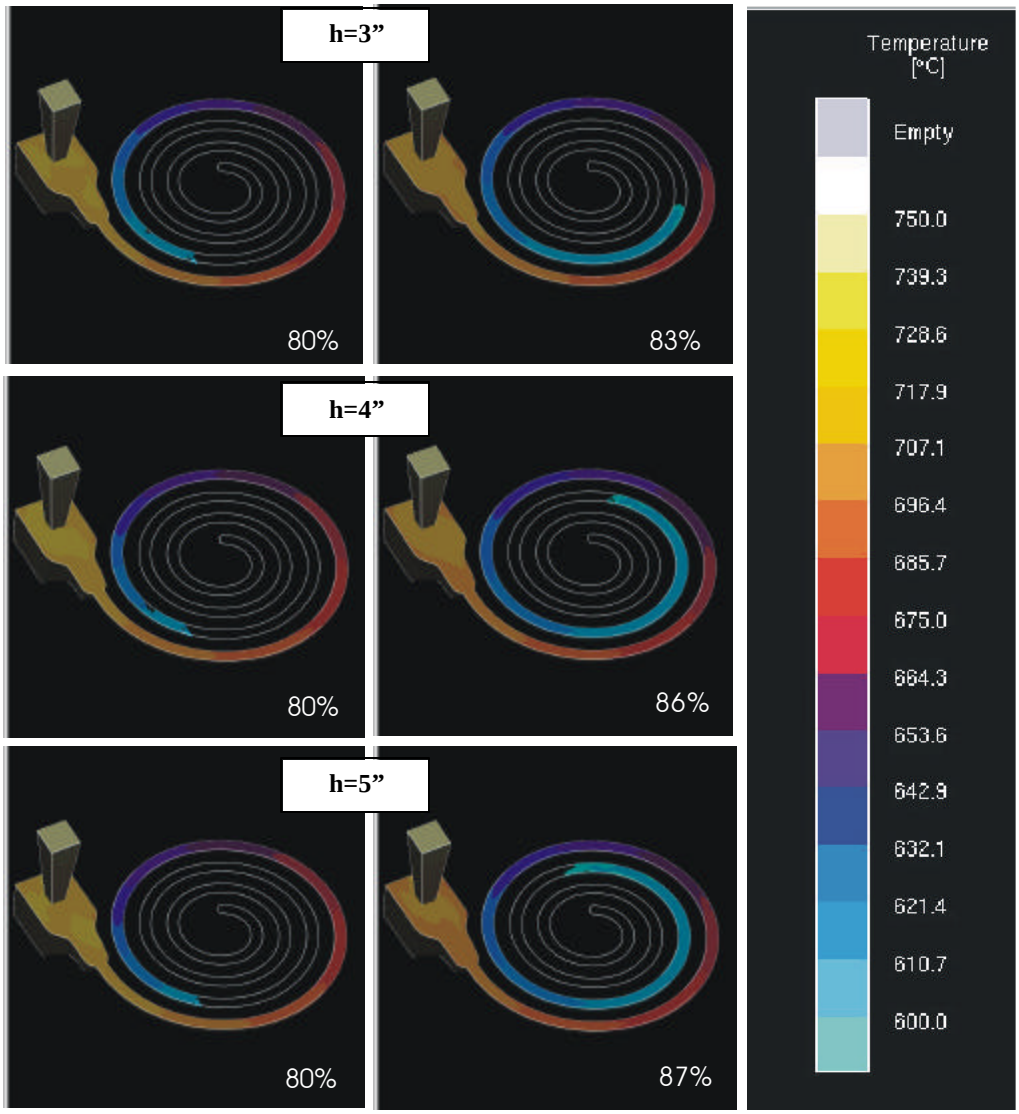

Figure 28: Head Pressure Sensitivity Temperature Fields for Fluidity Spiral

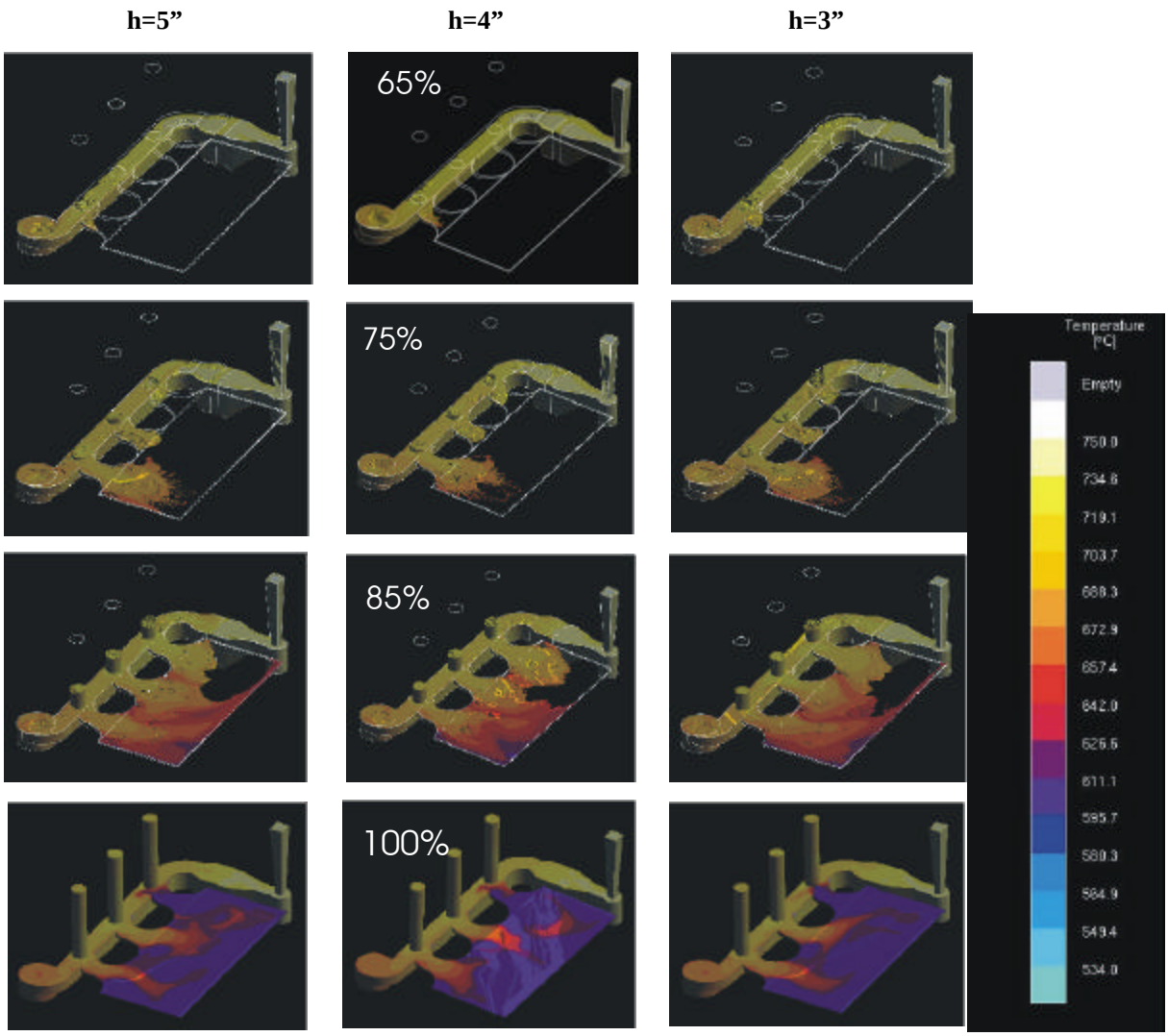

Figure 29: Head Pressure Sensitivity Temperature Fields for Thin Plate

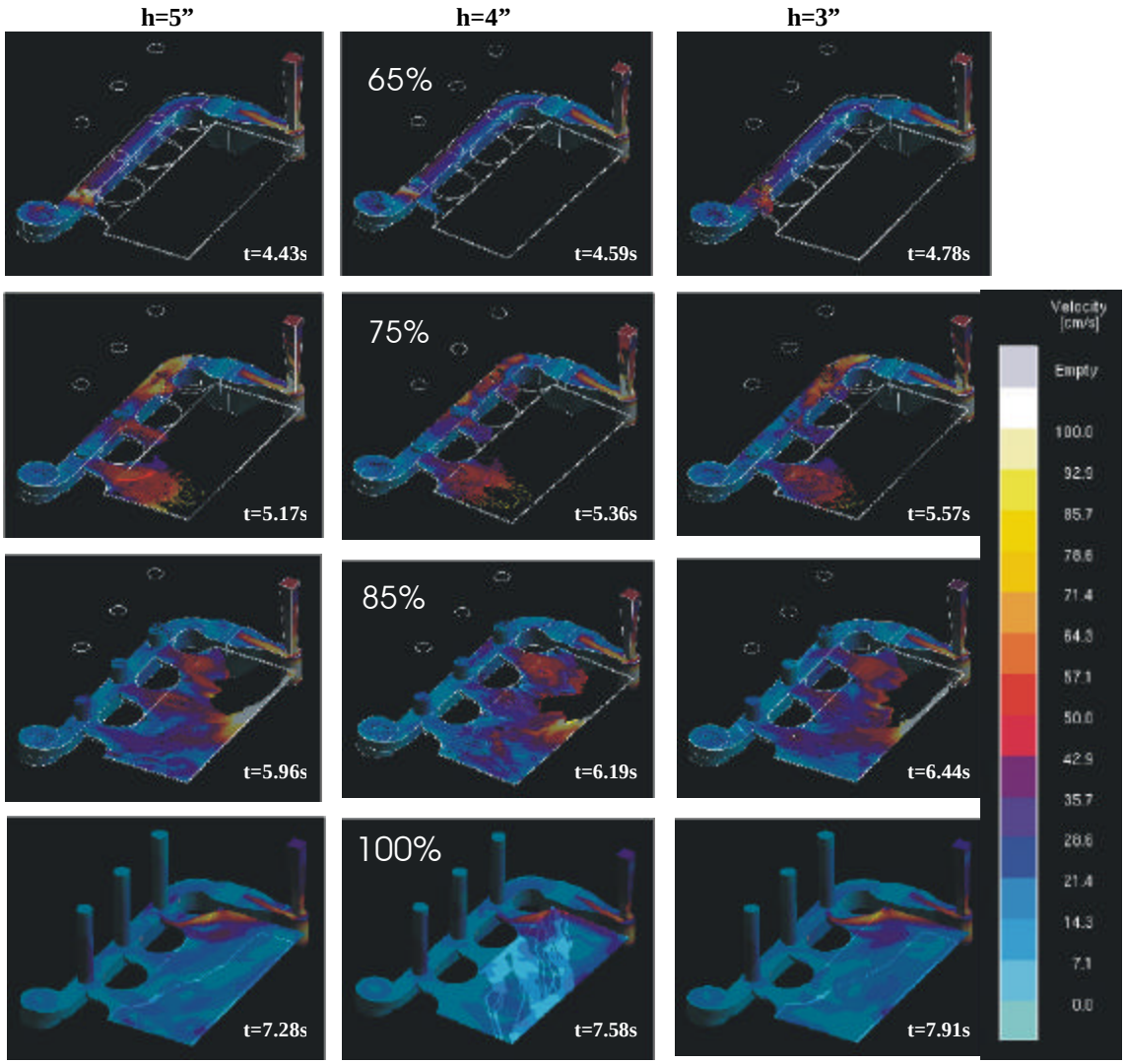

Figure 30: Head Pressure Sensitivity Velocity Fields for Thin Plate

Cooling Curves

Cooling Curves for the pouring basin sensitivity analysis can be found in Appendix A5.

Quantified Sensitivity Results

Figure 31 shows temperature and percent differences in fill for the spiral when the inlet head pressure boundary condition is varied +/-1”. It appears as though there is a increased temperature loss when the head pressure is decreased and a decreased

temperature loss when the head pressure is increased. It is thought that the increased velocities produced by a higher head pressure cut down on the time available for heat to leave the metal at a given point in the spiral. As far as ability to fill the spiral is concerned, it appears as though changing the head pressure +/-1" is about as influential as changing the thermal conductivity by +/-50%. Of course, there are different mechanisms at work giving similar results and the results point to the flow being the overwhelming phenomenon that is affected.

a. Metal Front Temperature Loss from Inlet to Probe # in Fluidity Spiral				b. Casting Percentage Filled at Flow Stoppage			
	h=3"	h=4"	h=5"		h=3"	h=4"	h=5"
#4 ΔT	**73.38**	**71.60**	**66.88**	% Filled	82.99	86.06	86.93
%difference	2.49%	----------	-6.58%	%difference	-3.57%	--------	1.01%
#6 ΔT	**140.97**	**139.27**	**132.58**				
%difference	1.22%	----------	-4.81%				

Figure 31: Quantified Pouring Basin Head Pressure Sensitivity Results for Fluidity Spiral

Figure 32 shows temperature and percent differences for the thin plate when the head pressure is varied. Notice how an increase in head pressure shows less temperature loss than a decrease. Also take notice that probe 7 ΔT in the h=5" case is shown in red. This temperature loss value of 111.67 is much higher than all other values. This is probably due to the altered flow that 5" of head pressure in the pouring cup produces. This value is not included in the -1.96% average difference as it is considered to be an outlier.

a. Metal Front Temperature Loss From Inlet to Probe

	Probe#	ΔT h=5"	ΔT h=4"	ΔT h=3"
Risers	1	**24.80**	**23**	**28.56**
	% diff	7.84%	-----	24.17%
	2	**24.04**	**25**	**22.70**
	% diff	-3.83%	-----	-9.18%
	3	**24.19**	**24**	**27.44**
	% diff	0.81%	-----	14.32%
Average		**24.35**	**24**	**26.23**
Avg % Difference		**1.44%**	**-----**	**9.30%**
Ingates	4	**33.36**	**36**	**36.91**
	% diff	-7.32%	-----	2.52%
	5	**42.99**	**46**	**50.46**
	% diff	-6.53%	-----	9.69%
	6	**41.91**	**54**	**42.62**
	% diff	-22.38%	-----	-21.06%
Average		**39.42**	**45.33**	**43.33**
Avg % Difference		**-13.03%**	**-----**	**-4.42%**
Plate	7	**111.67**	**60**	**59.32**
	% diff	86.12%	-----	-1.13%
	8	**66.14**	**73**	**91.76**
	% diff	-9.40%	-----	25.70%
	9	**67.20**	**71**	**62.57**
	% diff	-5.35%	-----	-11.87%
Average		**66.67**	**68**	**71.22**
Avg % Difference		**-1.96%**	**-----**	**4.73%**

b. Metal Front Temperature Loss From Ingate Probe 4 to Plate Probe 7

ΔT* between Probe 7(ingate) and Probe 4(plate)	h=5"	h=4"	h=3"
	78.31	24	22.42
% difference	**226.28%**	**-----**	**6.60%**
% of ΔT	70.12%	40.00%	37.79%

Figure 32: Quantified Head Pressure Sensitivity Results for Thin Plate

By varying the inlet head pressure of the system, there is a noticeable change in the amount of fill in the spiral. The velocity fields in the plate also show a slight change. The fluid flow is the mode of transport that is most affected by the change in head pressure.

4. Practical Applications

In the quest to make simulations of complex sand castings robust, the results of the sensitivity analysis were taken and utilized to validate simulation results with reality. To accomplish this objective, an experimental mold was instrumented with thermocouples in the same locations as Figure 5. The geometry of the real casting had slightly different risers from Figure 3 and is shown along with thermocouple locations in Figure 33. This thin plate was designed such that it produced a repeatable misrun shape in the plate region with typical casting conditions.

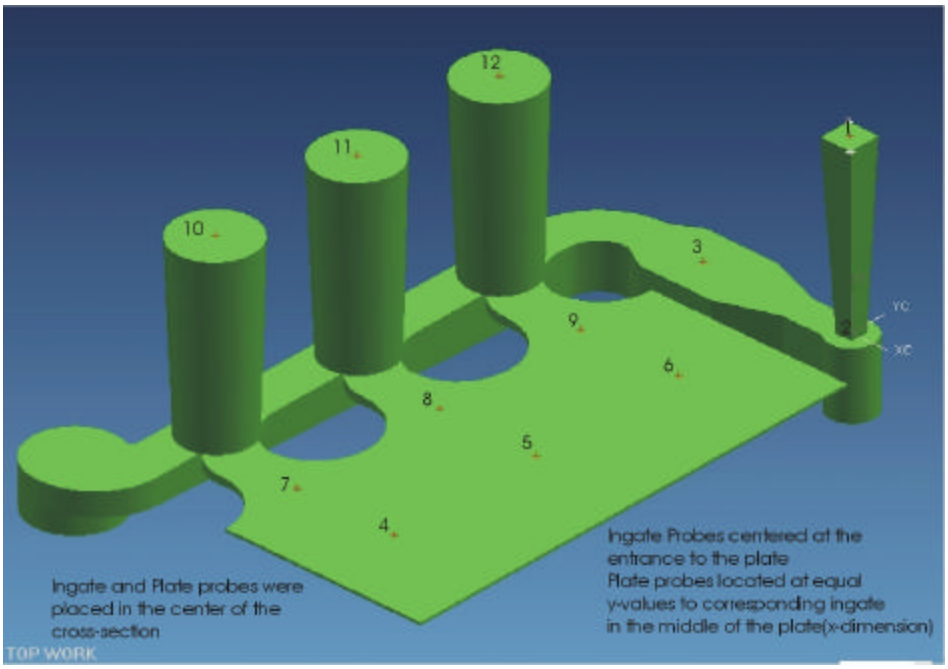

Figure 33: Misrun Plate Geometry with Thermocouple Locations

A sample was poured and cooling curves were collected throughout the fill at the locations of Figure 33. The aim of this exercise was to use the sensitivity analysis information in making the most appropriate changes to database values such that simulation generated cooling curves would match with experimentally measured cooling curves. Once this was

obtained, efforts were made reproduce the final misrun shape in the plate. A picture of the final casting is shown in Figure 34.

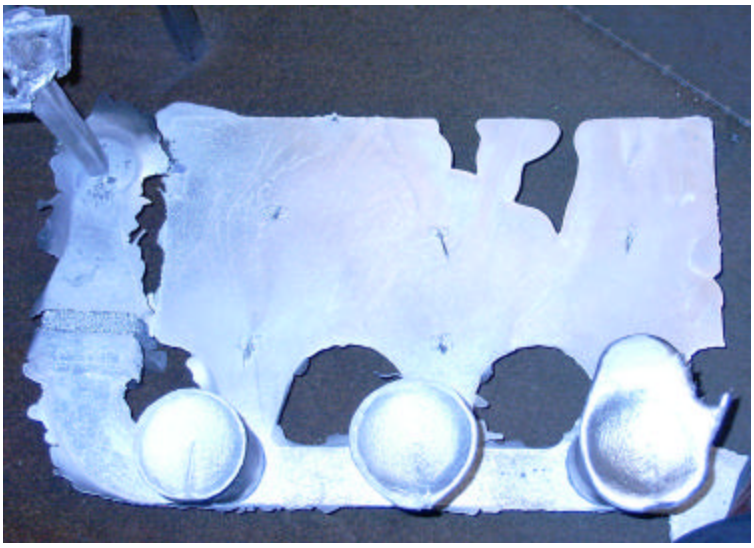

Figure 34: Misrun Plate Casting

Notice how the plate casting has a misrun in the center region.

Iteration 1

The first iteration simulation was performed using some of the default MAGMASOFT® database values and some values that were modified due to sensitivity analysis results. The rationale behind the modifications was as follows. In order to make the plate show a misrun, it was necessary to have plate temperatures go into the mushy zone to match experimental cooling curves. The inlet pouring temperature was measured and known, and was set at 720°C. The inlet head pressure was used as the flow boundary condition, which linearly decreased from 45 to 27 milibar over the 10 second measured pour time. Wall friction was turned on, giving a more realistic flow shape. All other values were from the default MAGMASOFT® database with the exception of the

alloy latent heat, which was adjusted from $436\,J/kg*K$ to a value of $390\,J/kg*K$ [2]. The most influential parameters were the mold metal HTC and the mold thermal conductivity as established by the sensitivity analysis. The HTC was adjusted to an abnormally high value of $3500\,W/m^2K$ and the thermal conductivity curve was multiplied by a factor of 2 to have a starting point at one extreme of database values. Upon performing the initial simulation, the plate produced only a slight misrun but cooling curves were below the experimental values. Figure 35 shows the temperature field of the completely filled plate with the small misrun in the corner.

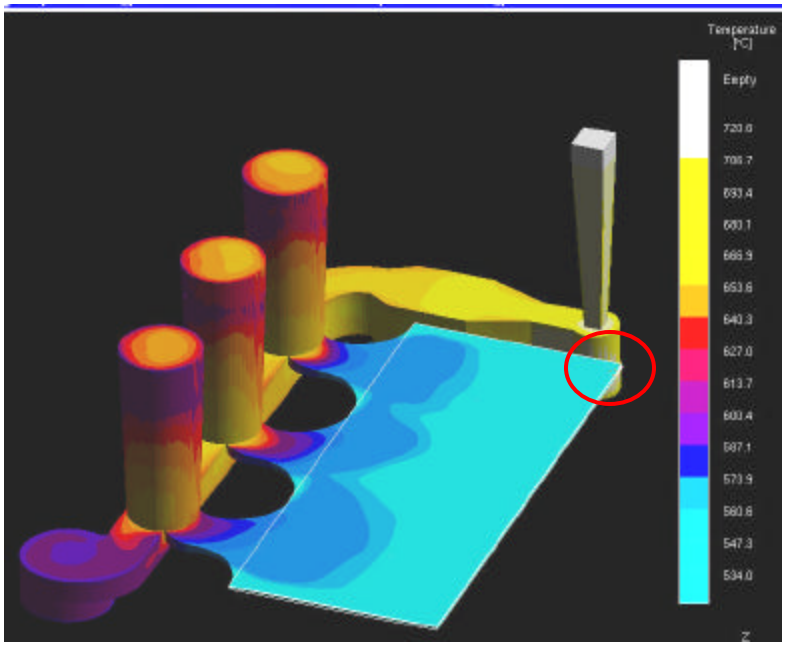

Figure 35: Iteration 1 Misrun Simulation

Figure 36 shows the cooling curves of Iteration 1 compared with experimentally measured values. Notice how the simulated curves are all below the experimental curves and the simulated misrun is much smaller than in reality. Since the default point of flow stoppage is 553°C or about 94% solid, it is not suprising that there is no misrun, since flow can stop

at much lower solid fraction values. This temperature for flow stoppage can be adjusted at any point to achieve the desired final fill pattern.

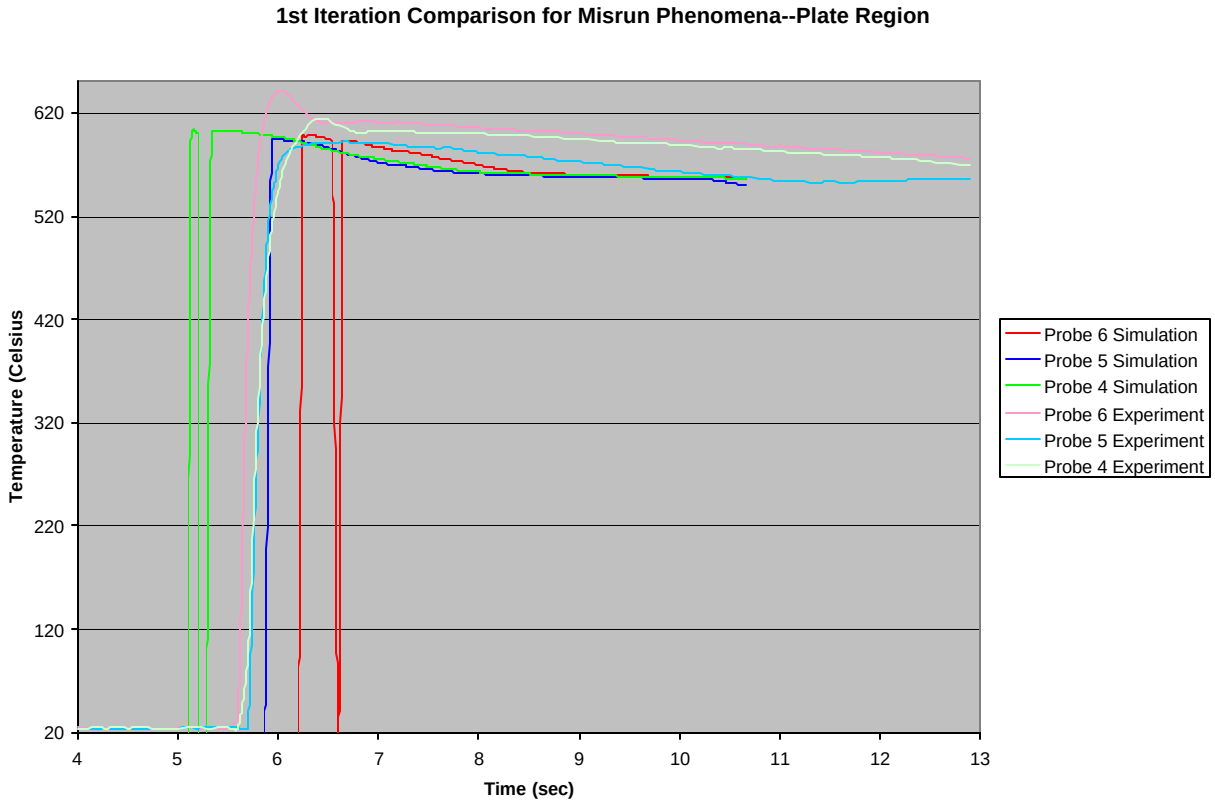

Figure 36: Experimental vs. Simulated Cooling Curves For Misrun Plate Iteration 1

Iteration 2

The next adjustment that was made was to lower the mold metal HTC to a realistic value of $1000 W/m^2 K$. This was done using the knowledge that the HTC is a key influential parameter in the filling of thin walled parts. The flow stoppage criterion was set to 565°C or about 50% solid fraction. Figure 37 shows the Iteration 2 temperature field with a slightly bigger misrun. Although it is still small and not in the correct location, the second iteration produces both a larger misrun and closer experimental cooling curve match. Figure 38 shows the experimental vs. simulated cooling curve comparison for Iteration 2.

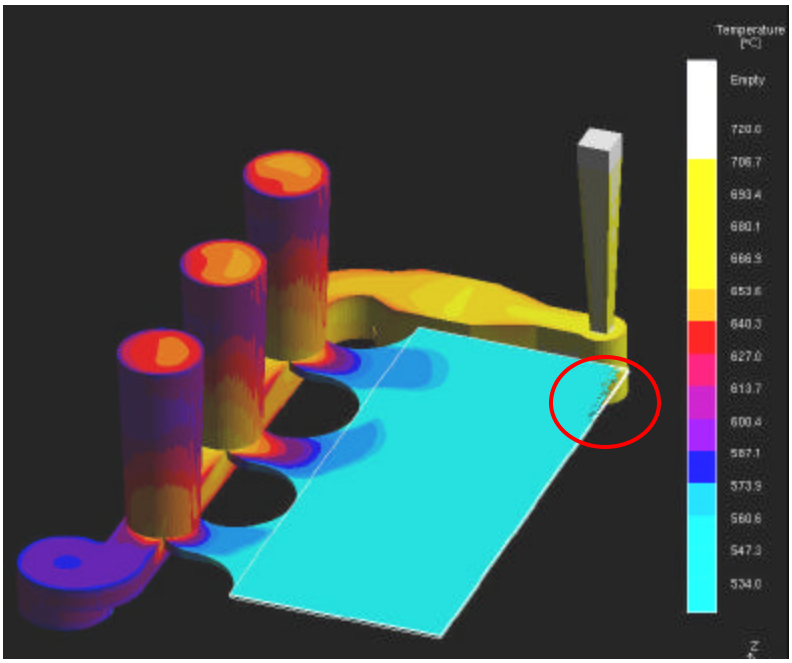

Figure 37: Iteration 2 Misrun Simulation

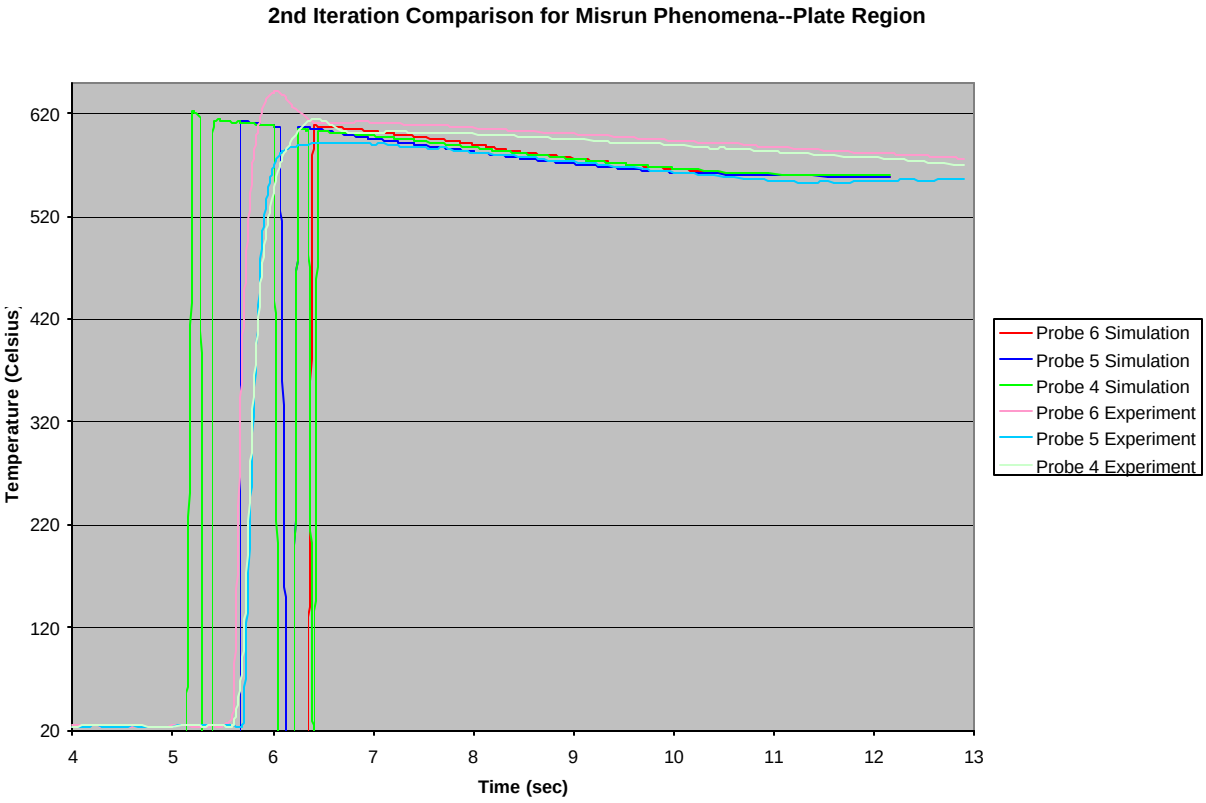

Figure 38: Experimental vs. Simulated Cooling Curves For Misrun Plate Iteration 2

Since Figure 38 shows all simulated cooling curves to fall within the bounds of the experimental curves, it was determined that for a first approximation, the cooling curves look to match well.

Final Iteration Results

Several more rounds of iterative adjustment of the flow stoppage temperature were performed until a temperature of 600° C was set. This corresponds to 25% solid fraction. The temperature field result at the end of this fill is shown in Figure 39. Notice the good correspondence with the shape and location of the misrun in the actual casting in Figure 34.

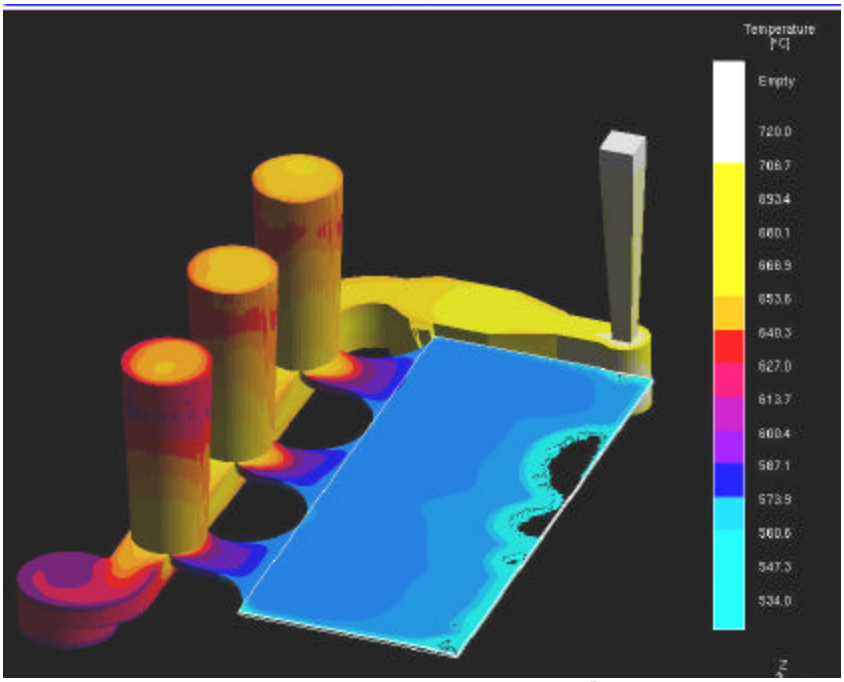

Figure 39: Iteration 6 Misrun Simulation

5. Benchmark Validation

The same material properties utilized on the final iteration of the misrun plate above were applied to a real, thin walled structural casting. A picture of the CAD model of the drawing with the green casting and gating and blue chills is shown in Figure 40. Default values were used to describe the alloy and chill properties.

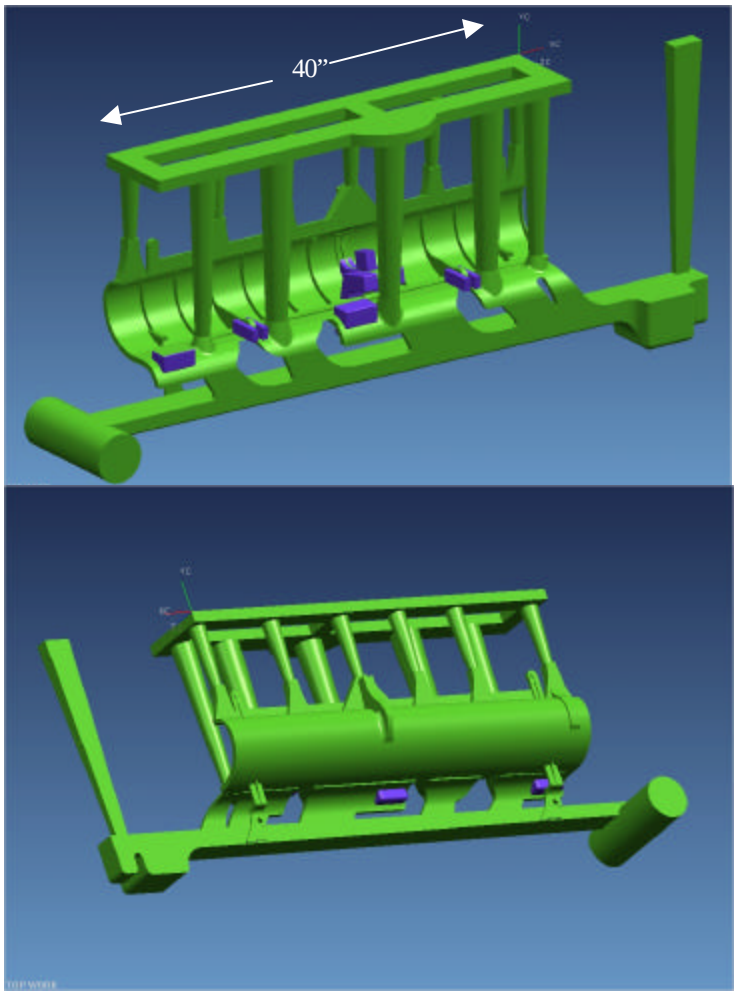

Figure 40: Benchmark Thin-Walled Casting Geometry

Information about the casting parameters is summarized in Appendix A6. Here is a brief list with the important parameters.

1. Production casting.
2. 92 million control volumes.
3. At least 2 control volumes across the thinnest wall.
4. Free-slip mold boundary condition.
5. Flow simulation depends on a 13 second fill time. This is the average fill time for production castings.
6. No filter model

This part has wall thicknesses as thin as 0.080" and has had a history of being scrapped due to misrun defects. Figure 41 shows a map of historical misrun defects on this casting.

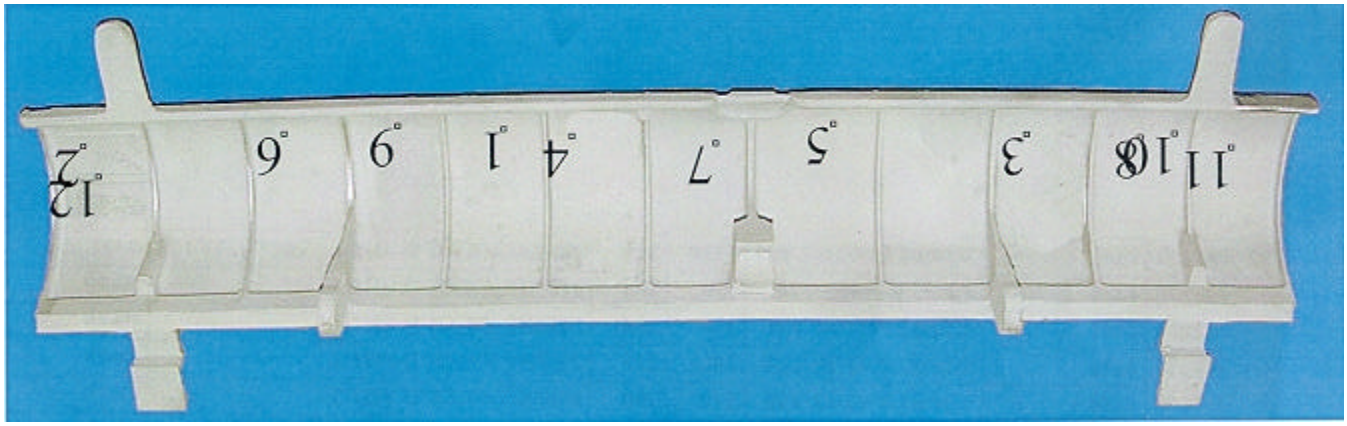

Figure 41: Misrun Defect History for Benchmark Casting

With adjustments made to the mold thermal conductivity and mold /casting HTC, it is expected that the correspondence noted in Figure 39 will also exist for the casting geometry here and produce results indicative of the defect history in Figure 41. A snapshot of the temperature field for the filled casting is shown in Figure 42. Notice how the simulation produces a misrun that is in one of the areas observed to coccur historically.

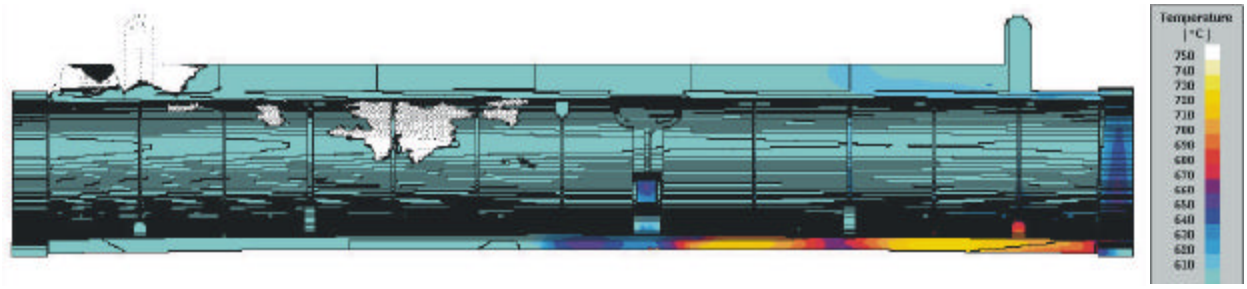

Figure 42: Benchmark Validation Simulated Misrun Defect

6. Conclusions

The results of this study point out several important issues, which are as follows. First, it is apparent from section 4 that the default database values may not be sufficient for use when modeling thin walled castings without a serious verification investigation. Specific foundry materials may exhibit quite different thermal behavior from experimentally measured generic materials in a laboratory. Once a non-correspondence is noted, it is necessary to identify the errant key parameter. Five of these key parameters were examined in this paper, mold-metal interfacial heat transfer coefficient, mold thermal conductivity, mold wall friction factor, pouring temperature, and pouring basin head pressure. It was determined that some parameters are more influential than others are, and their influences are often seen in temperature and velocity related results. For instance, pouring basin head pressure is a flow parameter and affects the amount of misrun in the fluidity spiral through flow characteristics. This is observable in velocity and flow results. Mold thermal conductivity, on the other hand, is a heat transfer parameter and affects the amount of misrun in the fluidity spiral through heat transfer characteristics. This is observable in temperature-related results. Both of these parameters contribute to producing a misrun. The most influential parameters are shown in Figure 43. These results are compiled from the temperature loss and percent filled results from the fluidity spiral.

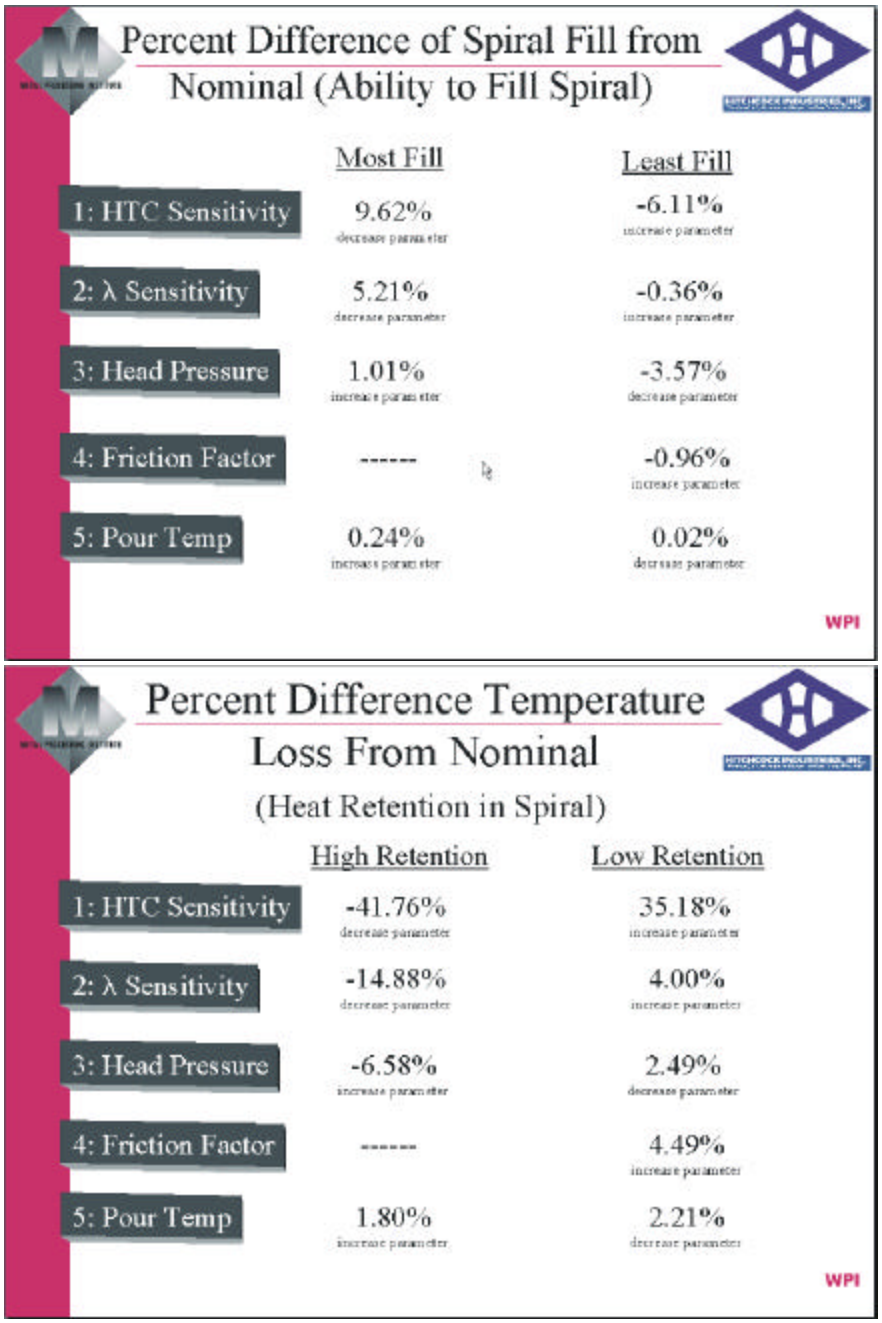

Figure 43: Most Influential Key Parameters

These key parameters are easily adjusted within the order of experimentally measured values to more closely match measured cooling curves. This was verified using simple test geometry, and validated using a real casting.

It is imperative that the reader must understand that this is only a first approximation at building a database of material properties for the thin-walled geometry castings. Modified values from section 4 were the mold-metal HTC, the mold thermal conductivity, and the flow stoppage temperature. It is expected that when thicker sectioned castings are encountered, a more precise manipulation of mold thermal conductivity will be necessary in accordence with the ideas outlined in section 2.1.4.

7. Recommendations for Future Work

Future work should involve addressing more of the key parameters, such as mold specific heat, and alloy thermophysical properties. The evaluation and specification of material properties should be undertaken with a variety of casting geometry and various alloys. The models going into producing results for porosity and microstructure should be investigated and specific material correlations should be established such as alloy feeding characteristics, and alloy microstructure with transient cooling conditions. With some of these issues resolved and their method of resolution established, the foundry will be more capable of tailoring a simulation tool to the materials and methods that are used on the shop floor. This will allow the foundry building these thin walled, structural parts to have a better, more accurate simulation tool to use to their advantage.

Appendix A1 Nominal Simulation Parameters

Thin Plate

PROTOCOL: HTC_sensitivity // version_1 // Page: 1

process : shape casting

calculations : filling

Mon Feb 25 10:45:50 CST 2002

New Project

Project Path: /home/joeyz/MAGMAsoft

Project Name: HTC_sensitivity

Project Version: v01

Master Project

Project Path: /home/joeyz/MAGMAsoft

Project Name: 9x21x09plate

Project Version: v03

MAGMA Structure

.../v01

.../v01/CMD

.../v01/SHEETS

.../v01/PAR

PROTOCOL: HTC_sensitivity // version_1 // Page: 2

material definitions

==========

	active in	database	file name	volume [cm^3]	start T [C]
Cast Alloy - 1	geom mesh	magma	AlSi7Mg06	387.16	750.00
Inlet - 1	geom mesh	magma	AlSi7Mg06	25.82	750.00
Feeder - 1	geom mesh	magma	AlSi7Mg06	679.26	750.00
Gating - 1	geom mesh	magma	AlSi7Mg06	2907.55	750.00
Ingate - 1	geom mesh	magma	AlSi7Mg06	171.08	750.00
Mold - 1	geom mesh	global	CBUMS-M-nom	182704.70	20.00
Insulation - 1	geom mesh	magma	Sleeve	1208.20	20.00
Filter - 1	geom mesh	magma	AlSi7Mg06	163.10	750.00

PROTOCOL: HTC_sensitivity // version_1 // Page: 4

mesh generation

==========

method : advanced

core generation : no

mesh advanced used for

Cast Alloy : ID 1

	mesh standard	mesh advanced
accuracy		
x	3	3
y	3	3
z	3	3
wall thickness		
x	5.00	2.00
y	5.00	2.00
z	5.00	2.00
element size		
x	5.00	1.00
y	5.00	1.00
z	5.00	1.00
smoothing	1.50	2.00
ratio	5.00	3.00

Number of CVs in x direction : 234

Number of CVs in y direction : 471

Number of CVs in z direction : 104

Total Number of CVs : 11462256

Number of Cast Alloy CVs : 398106

heat transfer definitions

	from (id)	to (id)	database	file name	group
1	Cast Alloy (1)	Mold (1)	magma	C1000.0	constant
2	Mold (1)	Insulation (1)	magma	C1000.0	constant
3	Mold (1)	Filter (1)	magma	C1000.0	constant
4	Mold (1)	Gating (1)	magma	C1000.0	constant
5	Mold (1)	Ingate (1)	magma	C1000.0	constant
6	Insulation (1)	Feeder (1)	magma	C1000.0	constant
7	Insulation (1)	Gating (1)	magma	C1000.0	constant
8	Insulation (1)	Ingate (1)	magma	C1000.0	constant

options

Sand Permeability : yes

Venting : no

Particles : yes

Shake Out : no

calculate erosion : no

storing data : percent

filling definitions

==========

active : yes

solver : 4

filling direction : neg. z

filling depends on : pressure

inlet 1

|time [s] |pressure [mbar]
-+---------+----------
| 0.00| 0.0000
-+---------+----------
| 0.10| 15.0000
-+---------+----------
| 0.30| 23.0000
-+---------+----------
| 0.50| 25.0000
-+---------+----------
| 10.00| 25.0000

filter definitions

|filter id | database/property | direction | active | group
-+----------+-------------------+------------+--------+-------
| [001] | magma/Foam_25ppi | x-direction | yes | Foam

|time [s] | percent [%]
-+----------+-------------
| | 10.00
-+----------+-------------
| | 20.00
-+----------+-------------
| | 30.00
-+----------+-------------
| | 40.00
-+----------+-------------
| | 50.00
-+----------+-------------
| | 60.00
-+----------+-------------
| | 65.00
-+----------+-------------
| | 67.50
-+----------+-------------
| | 70.00
-+----------+-------------
| | 72.50
-+----------+-------------
| | 75.00
-+----------+-------------
| | 77.50
-+----------+-------------
| | 80.00
-+----------+-------------
| | 82.50
-+----------+-------------
| | 85.00
-+----------+-------------

```
|       |       87.50
-+----------+-------------
|       |       90.00
-+----------+-------------
|       |       92.50
-+----------+-------------
|       |       95.00
-+----------+-------------
|       |       97.50
```

MAGMAfill (C) 1989- 2001

MAGMA GmbH
Kackertstr. 11
D-52072 Aachen
Germany

Ver.: 4.90

Current project path: /home/joeyz/MAGMAsoft/HTC_sensitivity/v01
PERMEABILITY mode activated
IINLST: 6786 elements allocated for mat.# 18

Creating ingate cross-section list

Creating ingate cross-section list

MATAIR has been assigned value of: 10 (16)
Defined are: 8 constant HTCs
Total of: 15 materials used (air included)
15 different material files used
Surroundings are automatically included

Approximate memory demand: 586.72[MBytes]

MATSCR: wrote 396756 elements to the disk file
Liquid metal will freeze at 25.0% of the solidification interval
Tfreeze decides upon solidification

Actual values of standarized HTCs
to the air: 50.0[W/(m2K)]
to the surroundings: 10.0[W/(m2K)]

FillRest will be invoked at: 98.0% filled

Free-slip boundary conditions on solid walls
Friction factor set to FRFACT factor set to: 0.00000
1 inlet materials defined in the mesh

1 inlet(s) are defined in the project file

Boundary conditions for the inlet # 1
Inlet B.C. type: user-defined pressure curve

Pressure: time-dependent curve defined
6 points on the curve defined

1	0.000	0.000
2	0.1000	15.00
3	0.3000	23.00
4	0.5000	25.00
5	10.00	25.00
6	0.1000E+06	25.00

The N-S solver (4) has been chosen
Material properties for the material # 1 (entry # 1) will be read
Default settings of the Tfreeze will be used
Ts= 534.00, Tl= 610.00, Tfreez: K0= 553.000, K1= 0.000 , K2= 0.000

Temperature driven freezing

Freeze temp., TFREEZ= 553.000

Average error of the computations estimated at: 0.70 percent

Spiral

PROTOCOL: f_s_htc_sensitivity // version_1 // Page: 1

process : shape casting

calculations : filling

_____

Tue Sep 03 14:37:25 CDT 2002

_____

New Project

Project Path: /home1

Project Name: f_s_htc_sensitivity

Project Version: v01

_____

Master Project

Project Path: /home1

Project Name: HTC_sensitivity

Project Version: v01

_____

MAGMA Structure

.../v01

.../v01/CMD

.../v01/SHEETS

.../v01/PAR

PROTOCOL: f_s_htc_sensitivity // version_1 // Page: 2

material definitions

==========

	active in	database	file name	volume [cm^3]
Cast Alloy - 1	geom mesh	global	357matwebk0TC	243.65
Inlet - 1	geom mesh	global	357matwebk0TC	4.37
Mold - 1	geom mesh	global	CBUMS-M-nom	3838.54

	start T [C]
Cast Alloy - 1	750.00
Inlet - 1	750.00
Mold - 1	20.00

cutbox factor : 1.00

Control Points

==========

Cooling Curve :

	Mat Gr	Mat Id	descr.	x	y	z
1	1	1	C1	0.71	86.51	76.20
2	1	1	C2	1.27	6.30	-7.37

3	1	1	C3	78.27	-101.15	-7.37
4	1	1	C4	195.72	-44.11	-7.37
5	1	1	C5	145.80	76.78	-7.37
6	1	1	C6	28.28	26.60	-7.37
7	1	1	C7	96.73	-81.52	-7.37
8	1	1	C8	175.35	13.14	-7.37
9	1	1	C9	57.20	34.69	-7.37
10	1	1	C10	129.37	-54.02	-7.37

Mat Gr	Mat Id	descr.	x	y	z
11	1	1	C11	85.01	31.56	-7.37

mesh generation

	mesh standard	mesh advanced
accuracy		
x	3	3
y	3	3
z	3	3
wall thickness		
x	5.00	1.50
y	5.00	1.50
z	5.00	1.50
element size		
x	5.00	3.00
y	5.00	3.00
z	5.00	3.00
smoothing	2.00	2.00
ratio	5.00	5.00

method : advanced

core generation : no

mesh advanced used for

Cast Alloy : ID 1

Number of CVs in x direction : 156

Number of CVs in y direction : 144

Number of CVs in z direction : 50

Total Number of CVs : 1123200

Number of Cast Alloy CVs : 40130

heat transfer definitions

==========

|from (id) |to (id) |database |file name |group

---+---+---+---+---+---

1| Cast Alloy (1)| Mold (1)| magma| C1000.0| constant

Appendix A2 Thermal Conductivity Sensitivity Cooling Curves

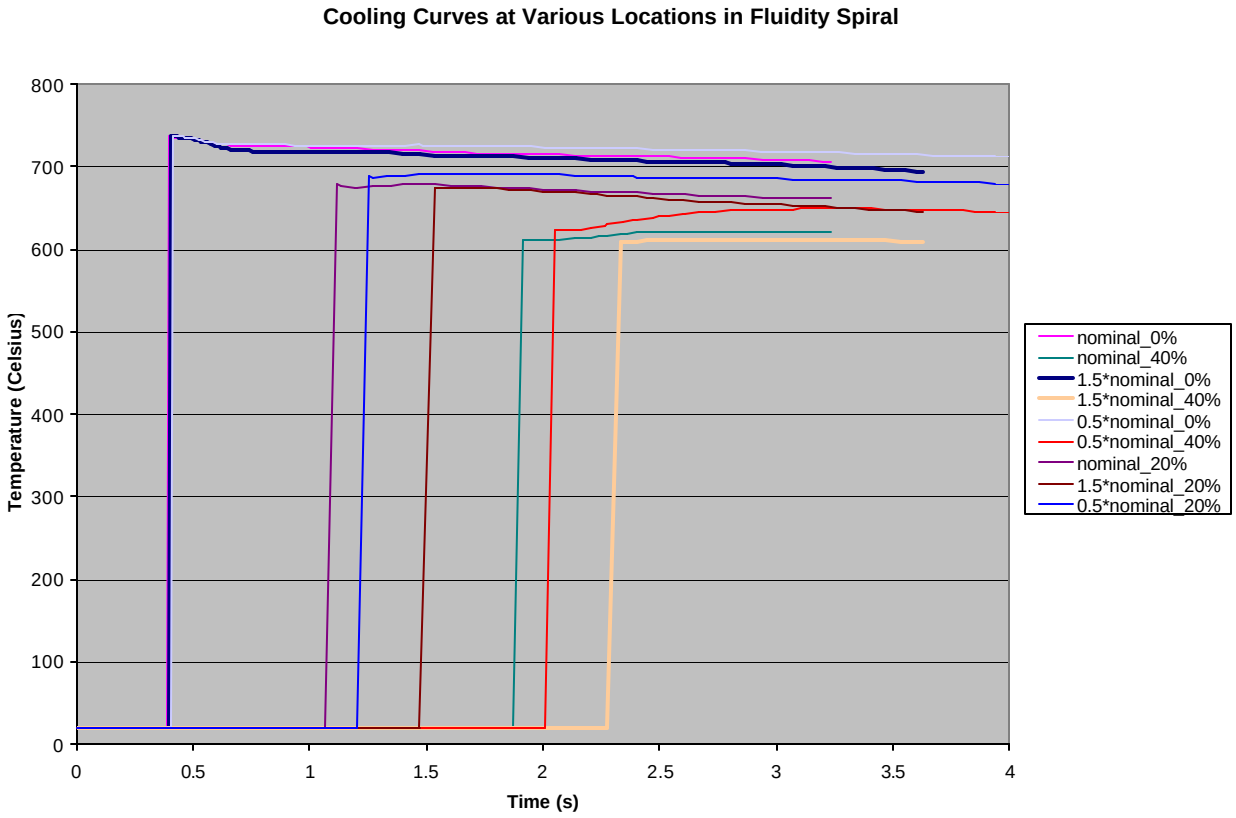

Figure 44: Thermal Conductivity Sensitivity Cooling Curves for Fluidity

a. Cooling Curves in Risers

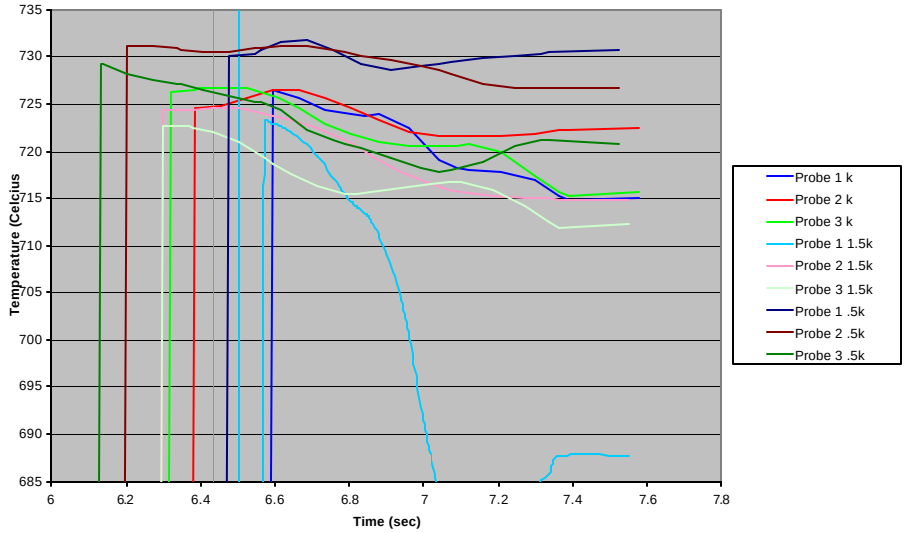

b. Cooling Curves in Ingates

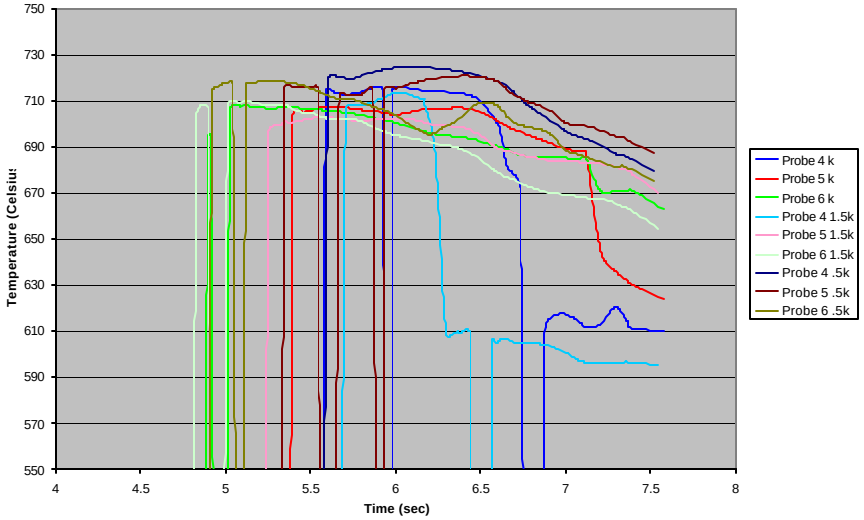

c. Cooling Curves in Plate

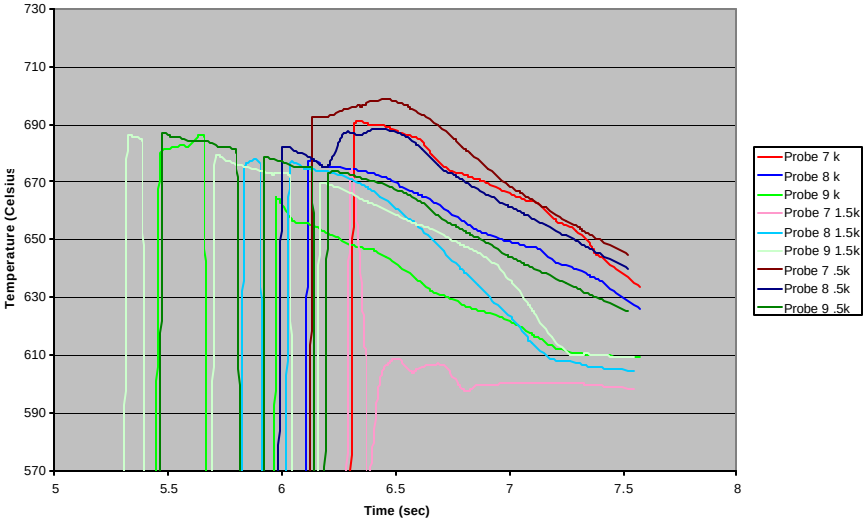

Figure 45: Thermal Conductivity Sensitivity Cooling Curves from Thin Plate

Appendix A3 Wall Friction Factor Sensitivity Cooling Curves

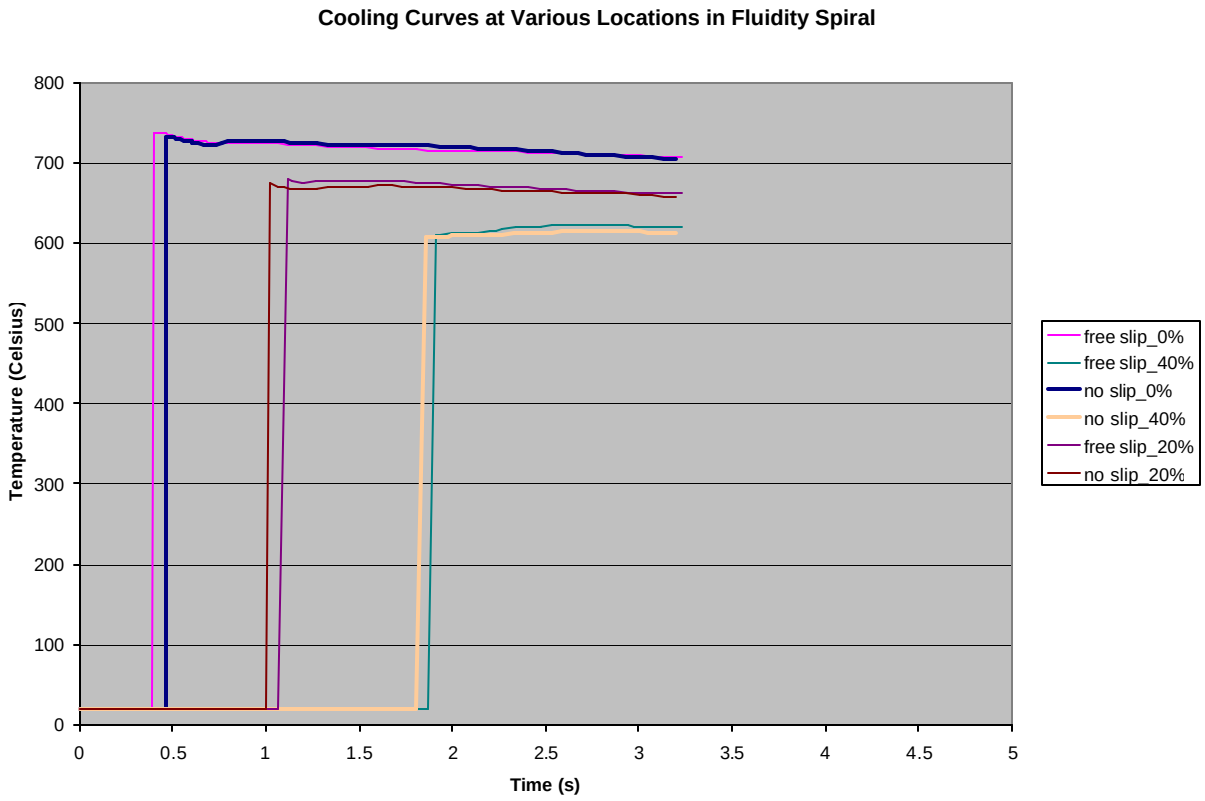

Figure 46: Friction Factor Sensitivity Cooling Curves for Fluidity Spiral

a. Cooling Curves in Risers

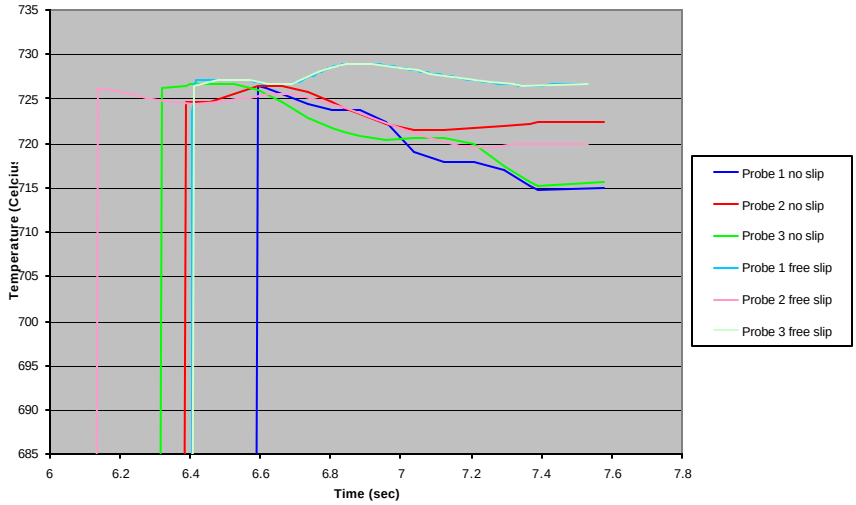

b. Cooling Curves in Ingates

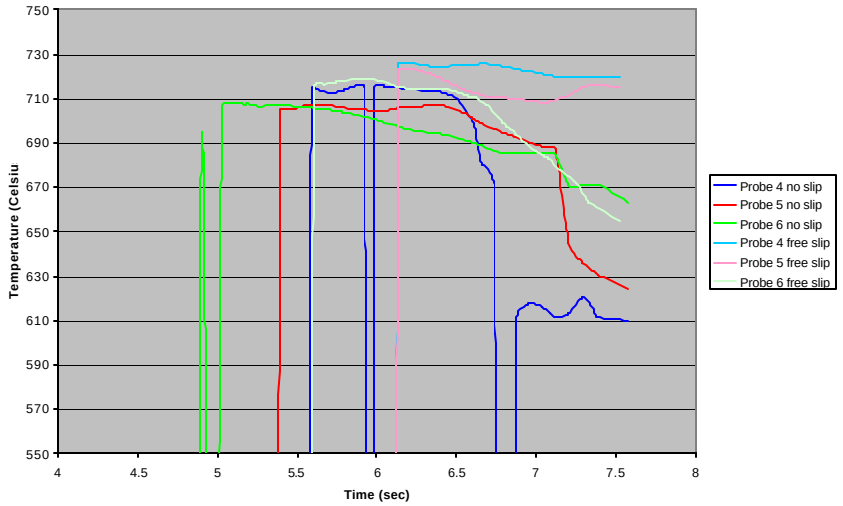

c. Cooling Curves in Plate

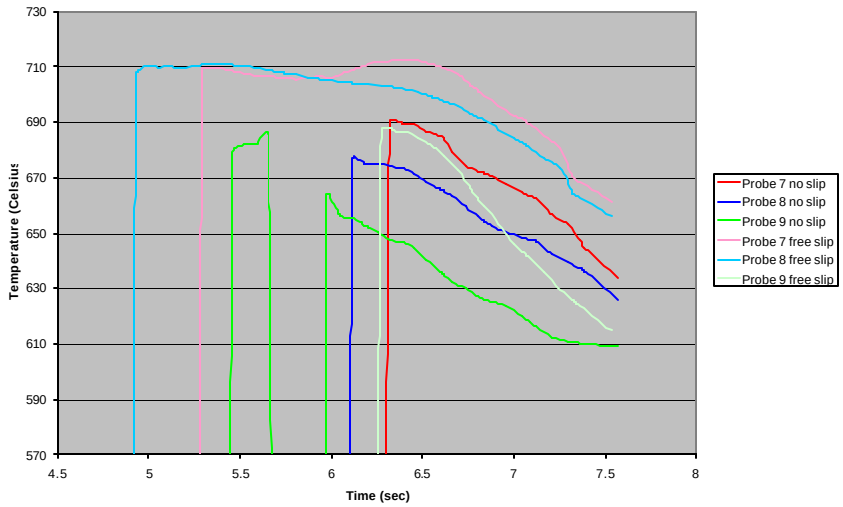

Figure 47: Friction Factor Sensitivity Cooling Curves from Thin Plate

Appendix A4 Inlet Pouring Temperature Sensitivity Cooling Curves

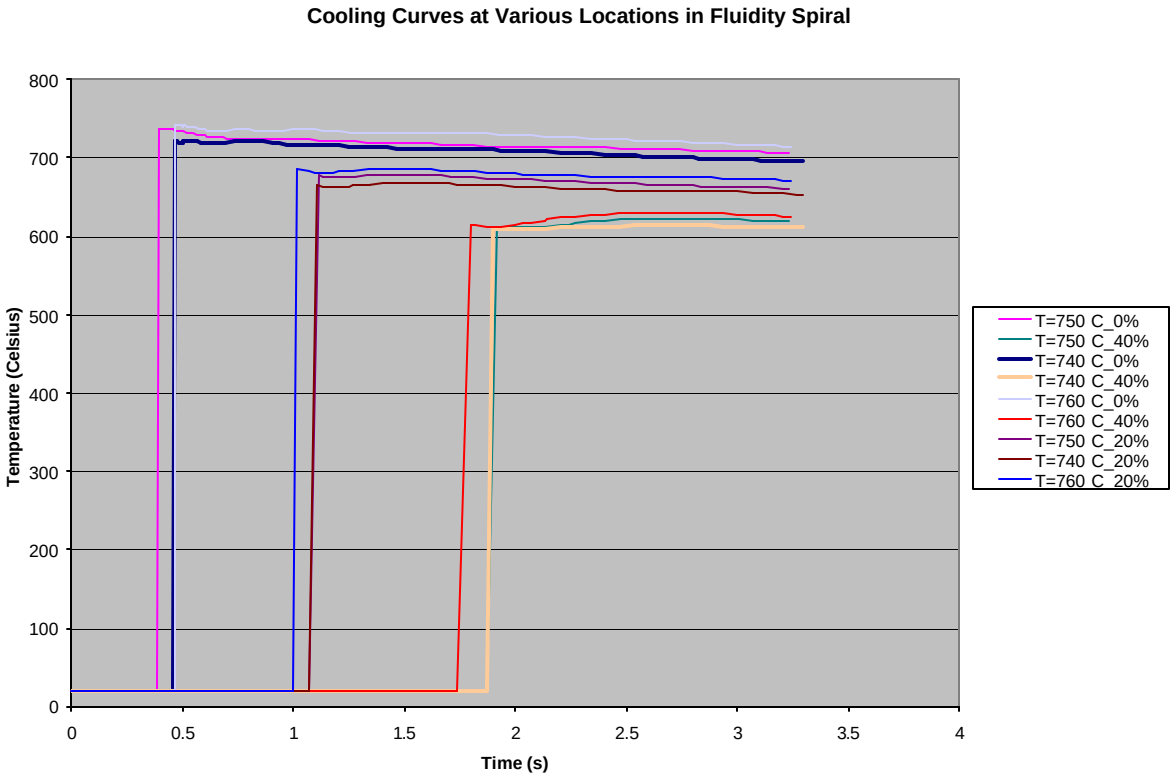

Figure 48: Inlet Pouring Temperature Sensitivity Cooling Curves for Fluidity Spiral

a. Cooling Curves in Risers

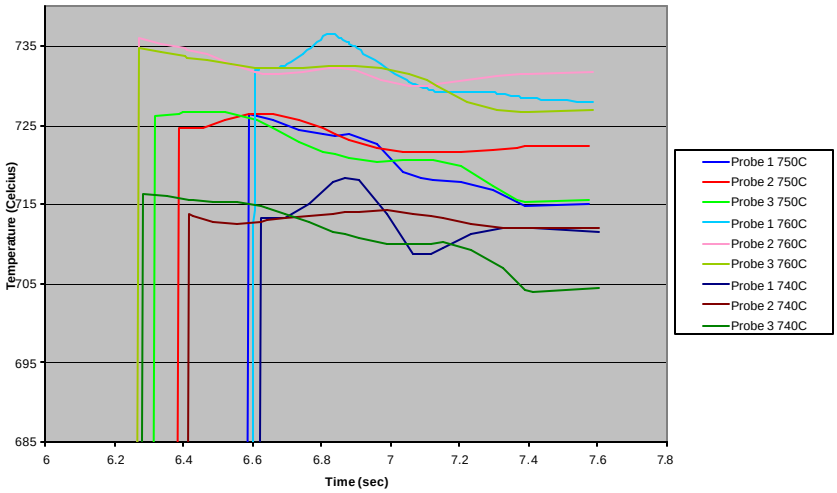

b. Cooling Curves in Ingates

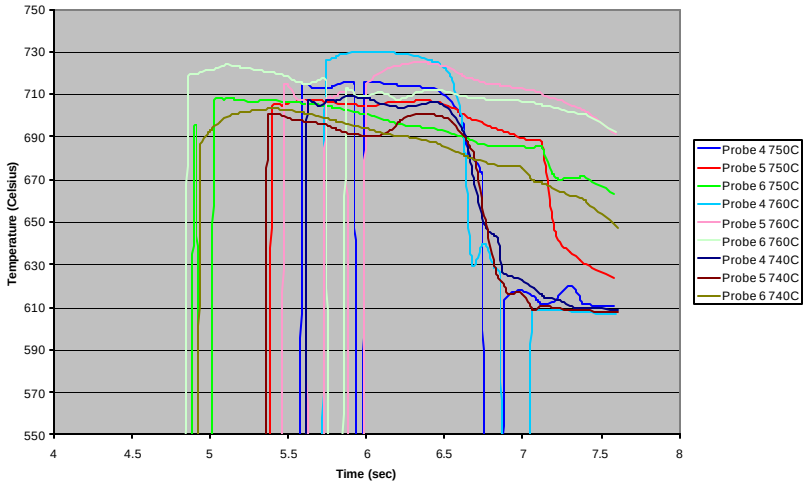

c. Cooling Curves in Plate

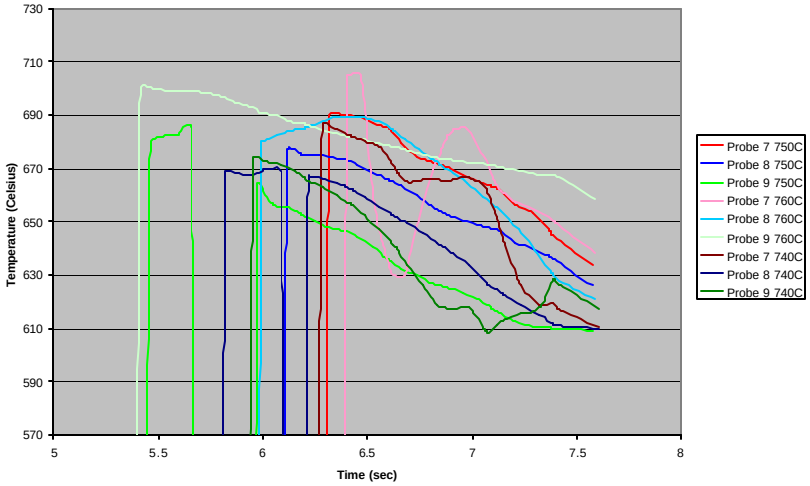

Figure 49: Inlet Pouring Temperature Sensitivity Cooling Curves from Thin Plate

Appendix A5 Pouring Basin Head Pressure Sensitivity Cooling Curves

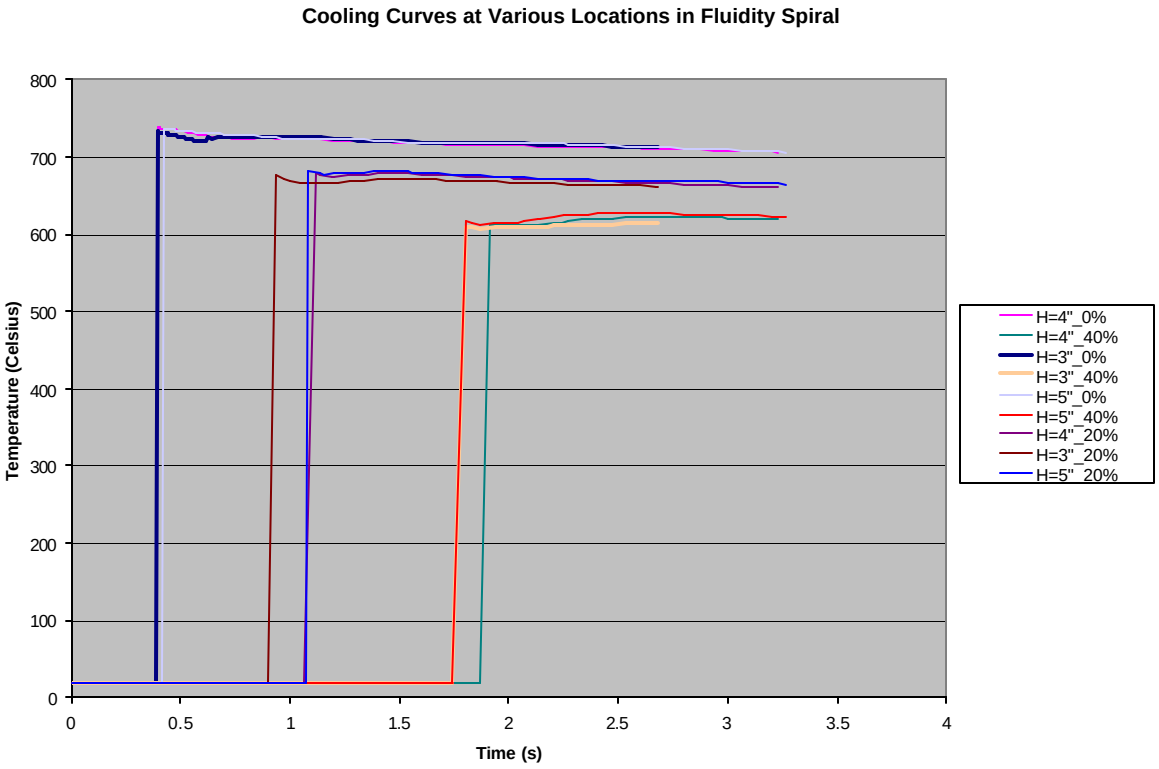

Figure 50: Pouring Basin Head Pressure Sensitivity Cooling Curves for Fluidity Spiral

a. Cooling Curves in Risers

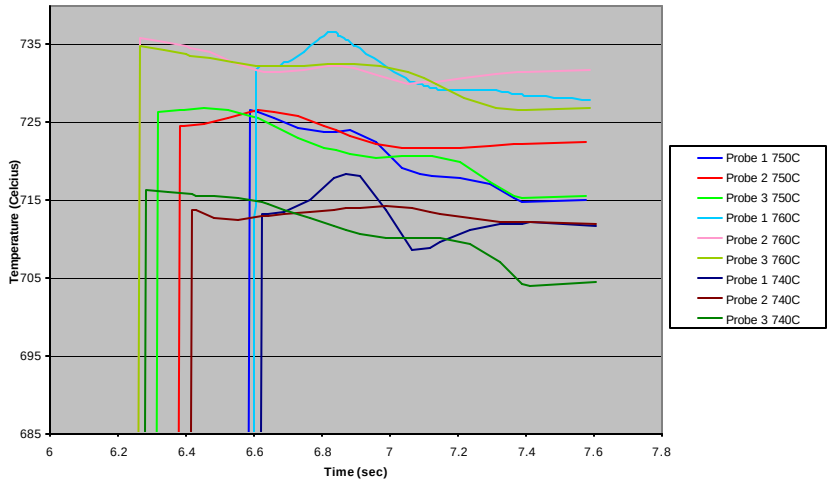

b. Cooling Curves in Ingates

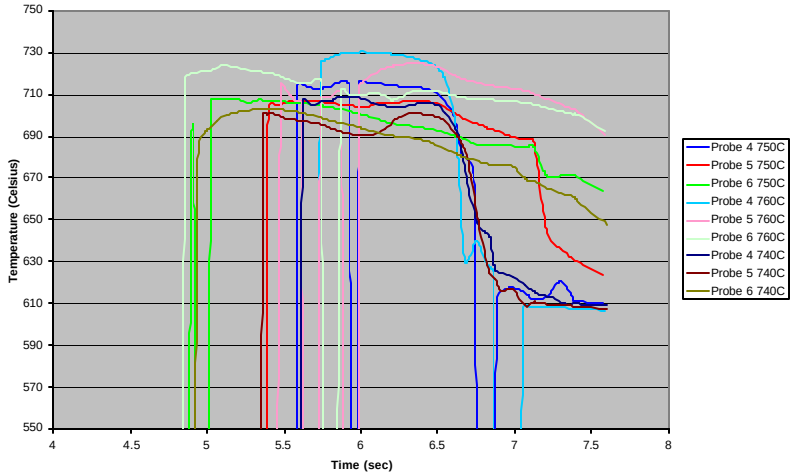

c. Cooling Curves in Plate

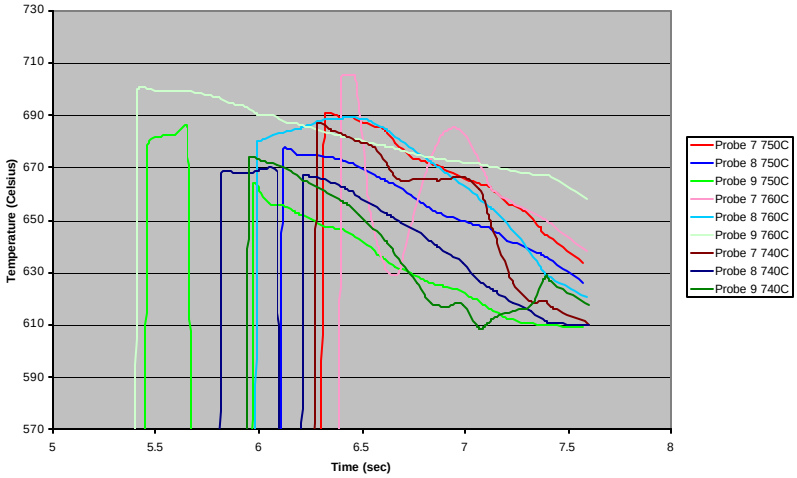

Figure 51: Pouring Basin Head Pressure Sensitivity Cooling Curves from Thin Plate

Appendix A6 Benchmark Casting Parameters

PROTOCOL: bullnose // version_2 // Page: 1

process : shape casting

calculations : filling, solidification

Mon Jul 08 15:48:04 CDT 2002

New Project

Project Path: /home/joeyz/MAGMAsoft

Project Name: bullnose

Project Version: v01

Empty Project

MAGMA Structure

.../v01

.../v01/CMD

.../v01/SHEETS

.../v01/PAR

Thu Aug 29 15:09:34 CDT 2002

New Version

Project Path: /home/joeyz/MAGMAsoft

Project Name: bullnose

Project Version: v02

Depends on: v01

Copy required files (+ mesh files)

PROTOCOL: bullnose // version_2 // Page: 2

material definitions

==========

	active in	database	file name	volume [cm^3]
Cast Alloy - 1	geom mesh	global	357matwebk0TC	1415.94
Inlet - 1	geom mesh	global	357matwebk0TC	45.34
Feeder - 1	geom mesh	global	357matwebk0TC	7076.67
Gating - 1	geom mesh	global	357matwebk0TC	9586.12
Mold - 1	geom mesh	global	CBMUS-M-nom-2.0k	241332.59
Chill - 1	geom mesh	magma	GrayIron_250	637.42
Filter - 1	geom mesh	global	357matwebk0TC	166.45

	start T [C]
Cast Alloy - 1	750.00
Inlet - 1	750.00
Feeder - 1	750.00
Gating - 1	750.00
Mold - 1	20.00
Chill - 1	20.00
Filter - 1	750.00

	y|	5.00|	3.00
	z|	5.00|	3.00
smoothing|	2.00|	2.00
ratio|	5.00|	5.00

cutbox factor : 1.00

PROTOCOL: bullnose // version_2 // Page: 3

mesh generation

Number of CVs in x direction : 933

Number of CVs in y direction : 251

Number of CVs in z direction : 393

Total Number of CVs : 92033919

Number of Cast Alloy CVs : 5077999

method : advanced

core generation : no

mesh advanced used for

Cast Alloy : ID 1

	|mesh standard	mesh advanced
accuracy|		
x|	3|	3
y|	3|	3
z|	3|	3
wall thickness|		
x|	5.00|	0.95
y|	5.00|	0.85
z|	5.00|	0.75
element size|		
x|	5.00|	4.00

PROTOCOL: bullnose // version_2 // Page: 4

heat transfer definitions

	|from (id)	to (id)	database	file name	group
1|	Cast Alloy (1)|	Mold (1)|	magma|	C1000.0| constant
2|	Cast Alloy (1)|	Chill (1)|	magma|	C1500.0| constant
3|	Mold (1)|	Chill (1)|	magma|	C1000.0| constant
4|	Mold (1)|	Feeder (1)|	magma|	C1000.0| constant
5|	Mold (1)|	Filter (1)|	magma|	C1000.0| constant
6|	Mold (1)|	Gating (1)|	magma|	C1000.0| constant

7	Chill (1)	Feeder (1)	magma	C1500.0	constant	
8	Chill (1)	Gating (1)	magma	C1500.0	constant	

References

[1] Flemings, M.C., *Solidification Processing*, McGraw Hill, 1974, ISBN 007021283X.

[2] *MatWeb Material Property Data,* Automation Creations, 1997, http://www.matweb.com/search/SpecificMaterial.asp?bassnum=MAC360.

[3] Pehlke, R.D., Jeyarajan, A., Wada, H., "Summary of Thermal Properties for Casting Alloys and Mold Materials", University of Michigan, NTIS -PB83-211003, December 1982.

[4] Midea, Tony, "Mold Material Thermophysical Data", 2002 *AFS Transactions* 02-080.

[5] Philipse, A. P., Schram, H. L., "Non-Darcian Airflow Through Ceramic Foams", Journal of the American Ceramic Society, v 74, pp 728-732, April 1991.

[6] Coury, J., "Permeability and Structure of Cellular Ceramics: A Comparison between Two Preparation Techniques", Journal of the American Ceramic Society, v81, pp3349-3352, December 1998.

[7] Magma Foundry Technologies, MAGMASOFT® v4.1 user's manual, 2001.